

SQUARE-WAVE OPERATION OF A THERMAL CONDUCTIVITY DETECTOR

by

SUNTAY HAYRI EDIZ

B. S., Wabash College, 1967

9984

A MASTER'S THESIS

submitted in partial fulfillment of the  
requirement for the degree

MASTER OF SCIENCE

Department of Chemistry

KANSAS STATE UNIVERSITY  
Manhattan, Kansas

1970

Approved by:

  
Major professor

LD  
2668  
T4  
1970  
E3  
copy 2

To My Parents

**ILLEGIBLE**

**THE FOLLOWING  
DOCUMENT (S) IS  
ILLEGIBLE DUE  
TO THE  
PRINTING ON  
THE ORIGINAL  
BEING CUT OFF**

**ILLEGIBLE**

**THIS BOOK  
CONTAINS  
NUMEROUS PAGES  
WITH DIAGRAMS  
THAT ARE CROOKED  
COMPARED TO THE  
REST OF THE  
INFORMATION ON  
THE PAGE.**

**THIS IS AS  
RECEIVED FROM  
CUSTOMER.**



## TABLE OF CONTENTS:

List of Figures . . . . .	iii
Introduction . . . . .	1
Literature Survey . . . . .	8
Construction . . . . .	15
Symbols . . . . .	17
Electronic Circuits . . . . .	18
Regulated Power Supply . . . . .	19
Smoothed High Current Supply . . . . .	22
Oscillator and Clamps . . . . .	24
Current Boosters and Common Mode Rejection Amplifier . . . . .	29
Preamplifier, Demodulator and Attenuator . . . . .	32
DC-AC Switching System . . . . .	35
Complete Circuit . . . . .	37
Bridge Control System . . . . .	40
Front Panel . . . . .	42
Parts List and Socket Pin Connections	
Regulated Power Supply . . . . .	44
Smoothed High Current Supply . . . . .	47
Oscillator and Clamps . . . . .	51
Current Boosters and Common Mode Rejection Amplifier . . . . .	54
Preamplifier and Demodulator . . . . .	58
DC-AC Switching System . . . . .	61
Parts List	
Bridge Control System . . . . .	64
Attenuator . . . . .	64

Operation . . . . .	65
Data and Discussion . . . . .	66
References. . . . .	69
Acknowledgement . . . . .	72
Vita . . . . .	73
Abstract	

## LIST OF FIGURES:

Figure 1	Graph of response of a detector vs. sample concentration. Relation between sensitivity and detection limit is shown. .	5
Figure 2	a. Schematic diagram of thermal conductivity detector powered by dc current. . . . .	6
	b. Schematic diagram of thermal conductivity detector powered by square-wave ac current. . . . .	6
Figure 3	Possible ac wave forms that may be used to power thermal conductivity detector. Relation between voltage and power is indicated. . . . .	7
	a. Sinusoidal ac	
	b. square-wave ac lacking vertical symmetry	
	c. square-wave ac lacking horizontal symmetry	
	d. symmetrical square-wave ac	
Figure 4	Katharometer cell designs. . . . .	10
	a. Flow-through	
	b. Convection-Diffusion	
	c. Self-purging	
Figure 5	Circuit diagram for regulated power supply. . . . .	20
Figure 6	Circuit diagram for smoothed high current supply. . . . .	23
Figure 7	Circuit diagram for oscillator and clamps. . . . .	26
Figure 8	Simplified schematic of clamping circuit. . . . .	27
Figure 9	Circuit diagram for current boosters and common mode rejection amplifier. . . . .	31
Figure 10	Circuit diagram for preamplifier, demodulator and attenuator. . . . .	34
Figure 11	Circuit diagram for dc-ac switching system. . . . .	36
Figure 12	Complete circuit; oscillator and clamps, common mode rejection amplifier and current boosters, dc-ac switching system, preamplifier and demodulator. . . . .	39
Figure 13	Circuit diagram for bridge control system. . . . .	41
Figure 14	Front panel of the instrument. . . . .	43
Figure 15	Etch pattern board I, foil side. . . . .	46
Figure 16	Etch pattern board II, foil side. . . . .	50
Figure 17	Etch pattern board III, foil side. . . . .	53

Figure 18	Etch pattern board IV, foil side. . . . .	57
Figure 19	Etch pattern board V, foil side. . . . .	60
Figure 20	Etch pattern board VI, foil side. . . . .	63
Figure 21	Results. . . . .	68
	a. Peak obtained with .2 $\mu$ l air sample when bridge was powered with ac current.	
	b. Peak obtained with 10 $\mu$ l air sample when bridge was powered with dc current.	
	c. Peak obtained with 10 $\mu$ l air sample when bridge was powered with ac current.	

## INTRODUCTION:

The measurement of thermal conductivity of gases goes back as far as 1840, but major studies have started early in the 20th century. In 1912, Langmuir<sup>1</sup> studied convection and conduction of heat in gases. Later in 1921, Shakespear<sup>2</sup> constructed an instrument to determine the purity of gas streams. He called his apparatus a "katharometer." In 1933, Daynes<sup>3</sup> published a book on gas analysis by thermal conductivity. In 1946, Claesson<sup>4</sup> measured the composition of binary and complex gaseous mixtures. Ever since, this method of analysis of gases has been employed as a major detection system in conjunction with gas chromatography.

Presently used thermal conductivity cells consist of four heat-sensing elements incorporated into a Wheatstone bridge circuit<sup>5</sup>, and positioned in a block made of aluminum, brass or stainless steel, heaters for the block, and a thermocouple to measure the temperature of this block. The heat sensing elements, which may be thermistors or resistance wires, are chosen so that their electrical resistance varies with temperature. They are placed in the separate cavities of the block, and heated by a constant current. Carrier gas must flow through these cavities whenever power is supplied, to prevent overheating of the filaments.

The temperature of the filaments reaches a certain constant temperature when the heat loss from the filaments to the carrier gas equals the heat supplied to the filaments from the power supply. Under these circumstances, the bridge output is adjusted to zero by means of one or more trimming circuits.

The heated filaments lose heat through radiation, conduction to the block through the thermal connections, forced convection and thermal

conduction to the gas stream. The latter two processes are usually dominant. If a carrier gas such as hydrogen or helium is used, then heat conduction due to gaseous conduction dominates. Heat loss is a complex phenomenon, and it is a function of bridge current, bridge resistance, thermal conductivity of sample gas and carrier gas, cell geometry, type and number of filaments.

The thermal conductivity detector is a concentration sensitive detector. It responds to those gases that have different thermal conductivities than that of the carrier gas. It would not differentiate between different species with nearly identical thermal conductivities, but it would produce an additive signal. Better sensitivity and better linearity are produced if a carrier gas of high thermal conductivity is used<sup>6</sup>. Of the two most highly conducting gases, hydrogen and helium, helium is used because it does not constitute an explosion hazard.

Since the stability of the detector depends strongly on detector temperature control, the detector block must be controlled within at least  $0.05^{\circ}\text{C}$ . The temperature throughout the detector block must also be uniform. Temperature changes at the filaments may be as small as  $10^{-4}^{\circ}\text{C}$ <sup>5</sup>.

Linearity of response over a wide dynamic range of sample concentration, Fig. 1, is one of the most important factors in the performance and evaluation of a thermal conductivity detector. Linearity of a detector largely depends on operating conditions. Sometimes, the manipulation of the detector parameters to draw linear graphs may tend to de-emphasize gross linearity errors<sup>7</sup>. The linear dynamic range of a thermal conductivity detector is  $10^4$ -fold (up to about 1%)<sup>5</sup>.

The detection limit, which is approximately 1 ppm for a conventional

thermal conductivity detector<sup>5</sup>, is defined as the sample concentration producing a signal equal to twice the noise level. Sensitivity and detection limit are related but they are not synonymous. The achievement of higher sensitivity does not necessarily mean a decrease in detection limit, since detection limit may be defined as  $2(\text{noise level/sensitivity})^8$ , Fig. 1.

When the sample gas elutes from the chromatographic column, it passes through the sensing elements of the detector, and less heat is transferred from the sensing elements. If the temperature of the block and the flow rate of the carrier gas are held constant, a change in temperature of the filament occurs, producing an unbalance in the associated Wheatstone bridge. This unbalance is recorded as a signal. As soon as the sample gas is removed from the hot sensing elements, the bridge returns to its original condition.

The Wheatstone bridge of the thermal conductivity detector is conventionally powered with a dc current. The output is then also a dc current which may serve as an input signal to a potentiometric recorder. Most recorders include an input chopper and ac amplification. With a conventional 1 mV recorder, it appears that the detection limit is controlled by the recorder, and not by the bridge<sup>9</sup>, Fig. 2a. Therefore it is apparent that a better read-out system is needed.

If a chopper is placed before the bridge, rather than at the output terminals, the bridge unbalance signal would be an ac signal of known phase and frequency, which could easily be amplified, after which noise signals could be rejected by means of synchronous rectification<sup>10</sup>. A major advantage of this approach is the elimination of critical low level choppers, and rejection of all thermal EMF's in the bridge circuit.

Accordingly, we decided to design and construct an ac bridge supply and output preamplifier to determine the detection limits attainable with such an instrument.

If varying current is applied to the elements of the bridge, problems such as thermal vibrations, and periodic magnetic interactions between the loops of the filaments may arise. This may not only damage the filaments, but it may also give rise to thermal noise.

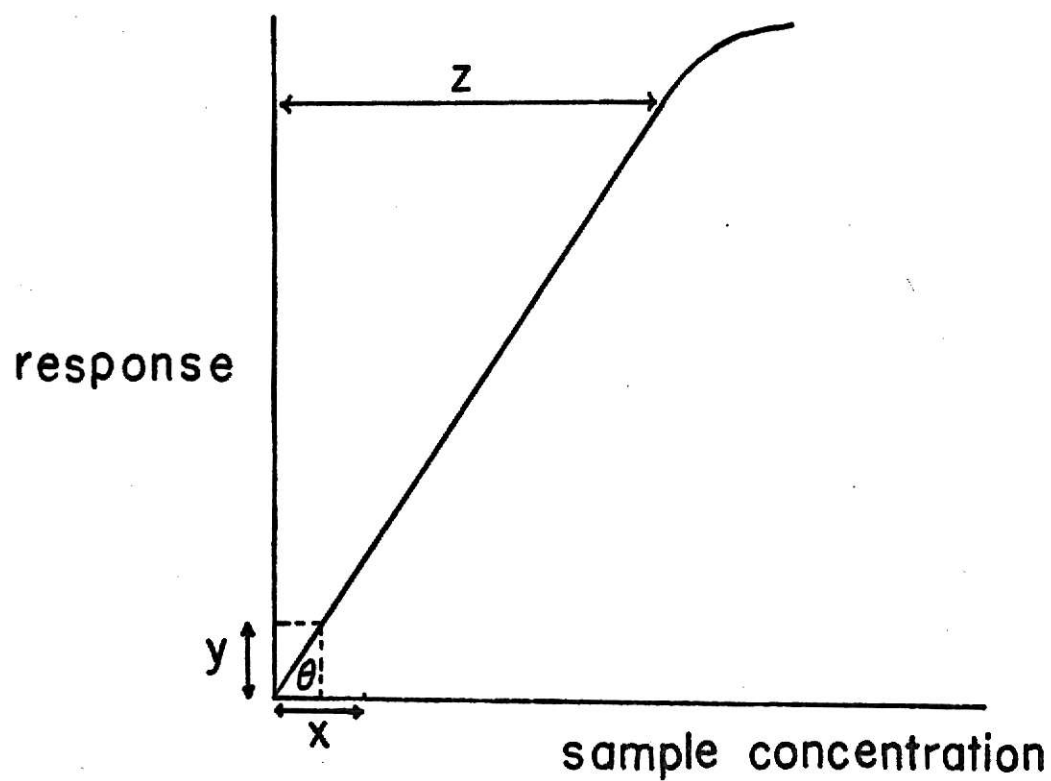
If the voltage supplied to the bridge is sinusoidal ac, power will vary as a function of time, since power is directly proportional to the square of the current. The filaments will heat up during the first  $1/4$  cycle and cool down during the next  $1/4$  cycle, Fig. 3a.

To eliminate the problems mentioned above, a perfectly symmetrical square-wave ac should be applied. This will result in constant power at the filaments at all times, Fig. 3d. The vertically dotted lines indicate the transients during the  $1/2$  cycles. Their effect may be made small enough to make any variations in power negligible.

If the square-wave ac lacks vertical symmetry, the power delivered to the filaments will have two distinct values during each cycle of the square-wave ac, Fig. 3b. Therefore, the vertical symmetry in the applied square-wave ac is crucial. If the square-wave ac lacks horizontal symmetry, the power at the filaments of the bridge will still be constant, Fig. 3c.

The upper two rows in Fig. 3 illustrate the considerations of the type of ac voltages applied at the inputs of the bridge. A and B have equal magnitude but they are out of phase by  $180^\circ$ .





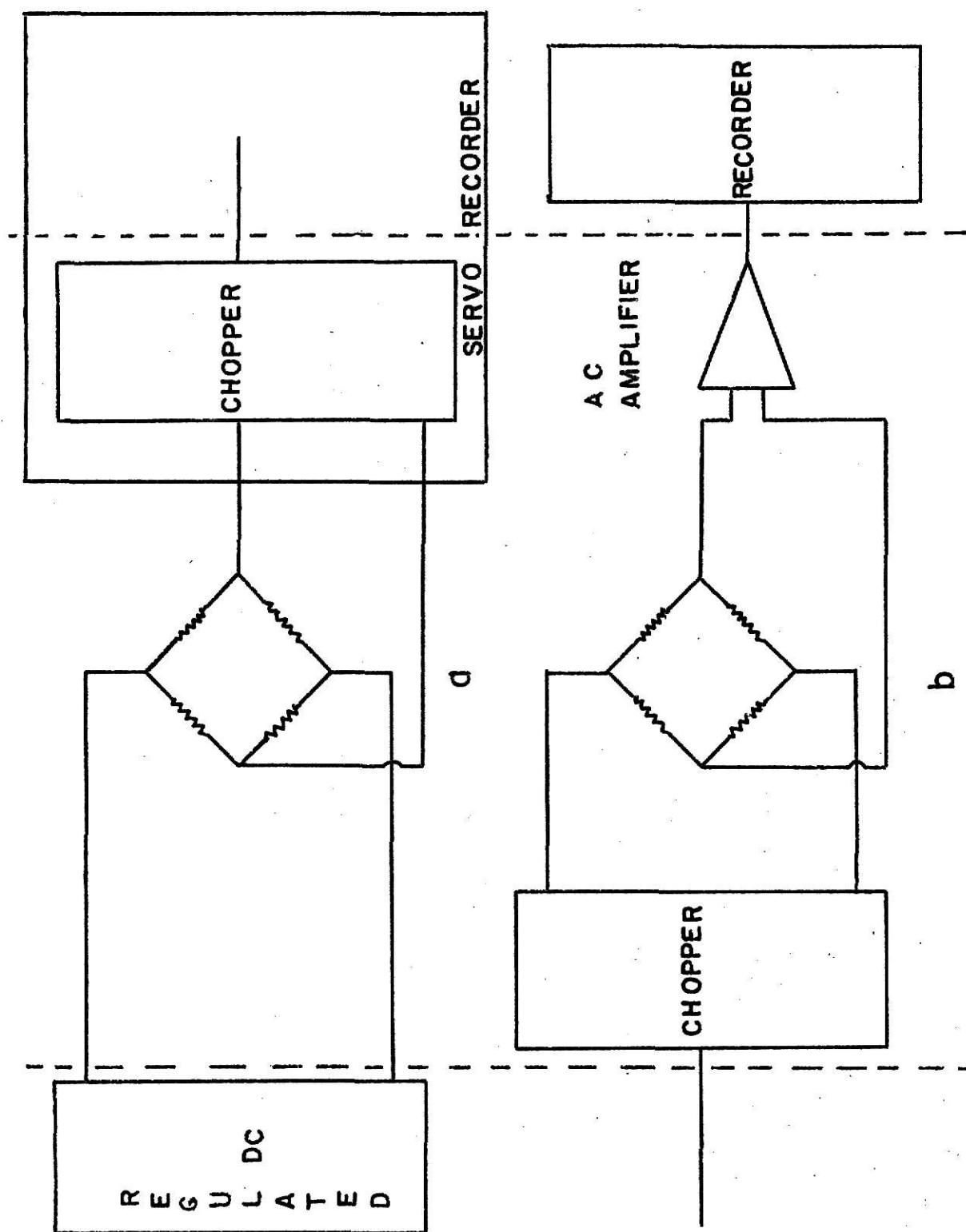
$z$ . dynamic range

$y$ . noise

$x$ . detection limit  $= 2y \cdot \cot \theta$

$\tan \theta$ . sensitivity

Fig.1



b Fig.2

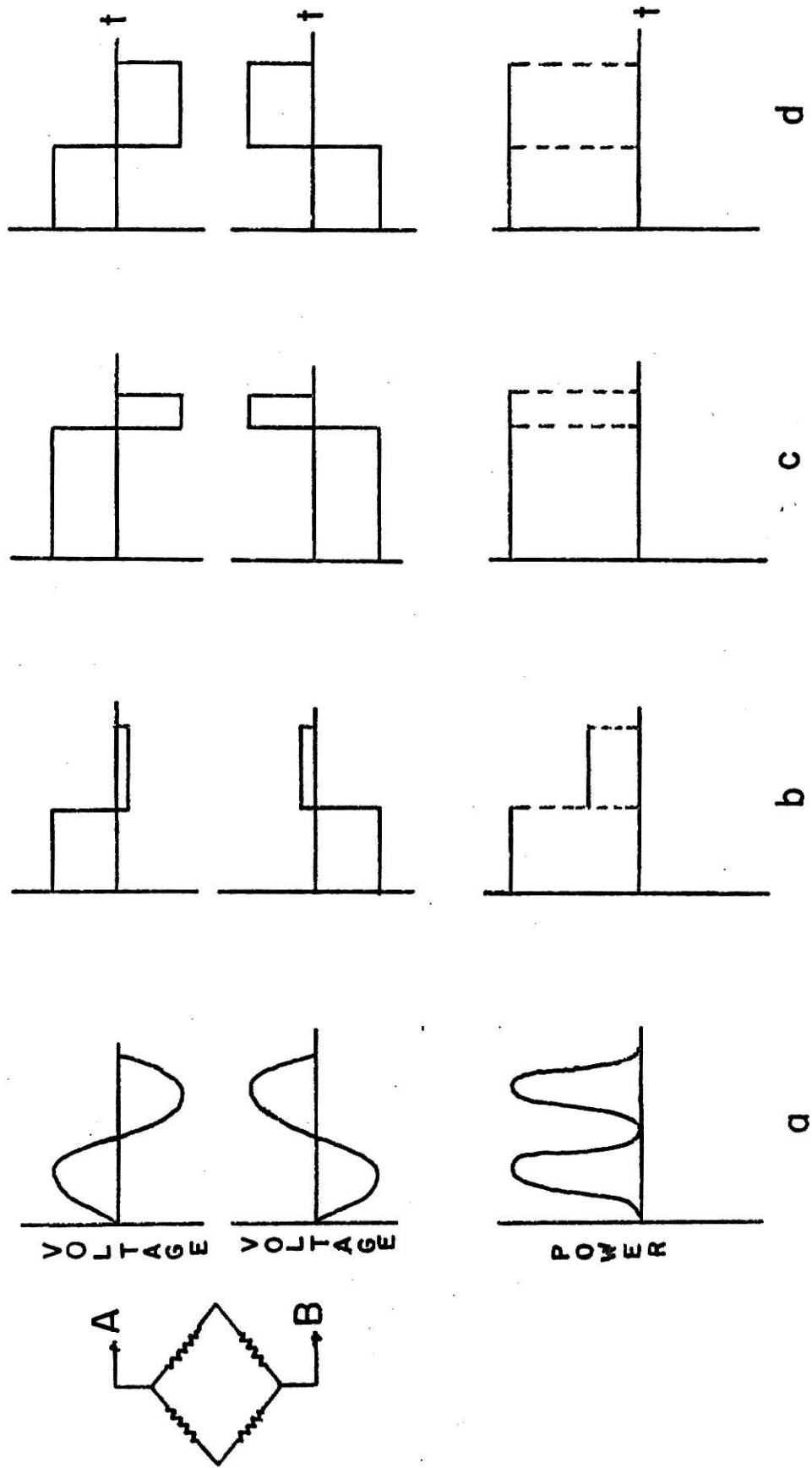


Fig.3

## LITERATURE SURVEY:

A number of investigators have studied the problems associated with enhancing the sensitivity and increasing the detection limit of the katharometer. They have attempted to achieve this through mechanical and electrical means.

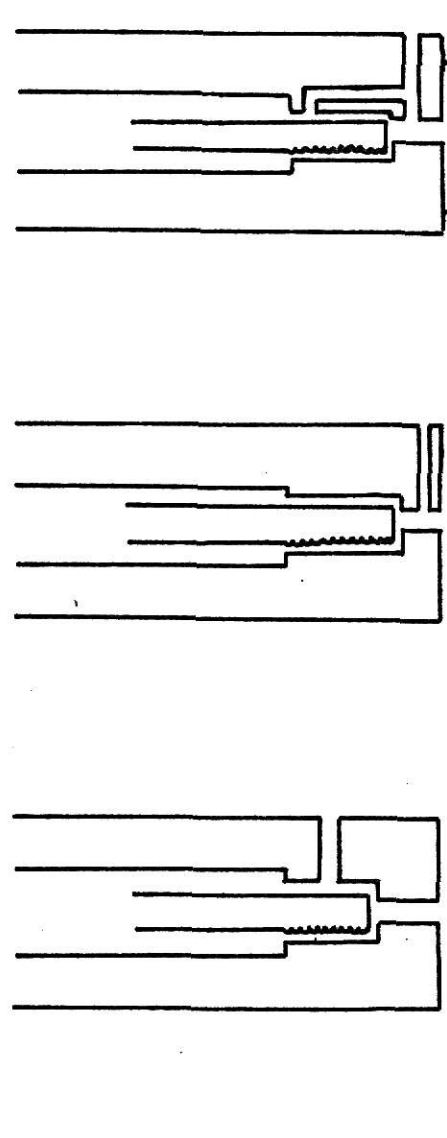
Extensive work has been reported by Keulemans<sup>11</sup>, who verified that the katharometer sensitivity was largely determined by the amount of current supplied to the sensing elements<sup>12</sup>, cell geometry<sup>13</sup>, thermal conductivity of the carrier gas<sup>14</sup>, and the temperature of the detector block<sup>15</sup>. Current increase, which causes a higher temperature difference between the sensing element and the detector wall, strongly influences the sensitivity, but baseline stability becomes a limiting factor as to the amount of current that can be employed<sup>11, 16, 17</sup>. Hoffmann<sup>18</sup> increased the temperature gradient by cooling the block, rather than increasing the filament temperature. Increase in current has another drawback: catalytic reactions may occur at the filaments at higher temperatures when H<sub>2</sub> is used as a carrier gas. This results in fouling of the sensing elements, whose sensitivity is thereby masked to a great extent<sup>11, 12</sup>. This problem can be eliminated by coating the sensing elements with glass. Under these circumstances, good sensitivity, low drift, reasonably fast response, and high mechanical stability of the sensing elements have been reported<sup>19, 20</sup>. Obermiller et.al.<sup>21</sup> have clad the tungsten filaments with Teflon, and proved that they were far superior to the bare tungsten filaments. A non-corrosive thermal conductivity cell made out of glass or quartz has also been reported, with its sensing elements surrounded by a tightly packed aluminum powder<sup>22</sup>.

It has been shown that a direct relationship exists between the design of the cell or cell geometry, the location of the filaments in the cell with respect to the gas stream, and the flow sensitivity of the time constant or response time of the detector<sup>8,23</sup>. Of the three types of cell designs which are illustrated in Fig. 4, the self purging produces the best time constant, which is directly proportional to the volume, and a low flow sensitivity. With the modified design of diffusion-type four-filament cell, the signal is independent of flow rate fluctuations at flow rates higher than a certain minimum value<sup>24</sup>.

Soma et al.<sup>25</sup> have achieved lower detection limits with thermistor sensors. They enclosed one of the sensing elements in a cavity covered with a membrane permeable to gases, while the other one was contained in a cavity covered with an impermeable membrane. These authors obtained rapid response time and noted a decrease in detection limit due to self-heating effect of the thermistors with currents of about 2 mA. Temperature differences were measured with a differential amplifier; the noise level was less than 0.1  $\mu$ V.

Sensitivity of the filaments has been found to be roughly proportional to the product of the resistivity,  $\rho$ , and the square root of the temperature,  $T$ , of the wire. Platinum and tungsten are the most popular metals used for the sensing elements. Bismuth and antimony have the highest product of the two properties mentioned above, but unfortunately these metals cannot be drawn into wire<sup>11</sup>.

The use of V-shaped filaments to achieve higher sensitivity has been reported in the literature<sup>26</sup>, but the most common design has been the helical type which permits the insertion of long wires into the small bores of the detector block<sup>11</sup>. Different sensitivity values have been reported



a. flow-through      b. convection-  
diffusion      c. self-purging

# KATHAROMETER CELL DESIGNS

Fig. 4

for filaments coiled into single and double helices<sup>27</sup>.

Efforts have been made to minimize the dependence of the sensitivity on the flow of the gas stream. Two fine metal screens have been wrapped around the thermistor bead. The inner screen decreased the effect of the gas flow at least 10-20 fold, while the second screen eliminated the effects arising from mechanical vibrations. The transient output of the detector at the time of sample introduction was 20  $\mu$ V compared to 2 mV for the unscreened thermistor. When another screen was added, the response to the pressure transient on injection was 1  $\mu$ V<sup>28,29,30</sup>. Modell<sup>31</sup> placed the sensing element, a thermistor or a hot wire, in the center of a cylindrical screen bed packed with hollow glass spheres, particle size of about 30-125  $\mu$ . The sensing element then was placed perpendicular to the gas stream. The reference element was supplied with gas from an independent source. The author reported that sensing elements became relatively insensitive to flow above gas velocities of 30 cm/sec. The response time of the packed-bed sensing elements was 1.5 times that of the screened thermistor at high flow rates. The noise level in laminar flow was not measured. In turbulent flow, the packed-bed is superior; noise level was about 0.2 mV because turbulence cannot penetrate the packed-bed, and only heat loss from the screen varies. This variation becomes unimportant as thermal resistance from the screen decreases with increasing flow rate.

Better detection limits are also attainable through proper modifications of the power supply to the thermal conductivity cell, mechanical variation of the Wheatstone bridge, and handling of the output signal. Hannah<sup>32</sup> replaced the zinc-carbon 9-volt dry cell battery with an 8.4-volt nickel-cadmium battery. The latter is advantageous in that it supplies

steady power and it is rechargeable. Littlewood<sup>33</sup> connected a resistor in parallel with the sensing elements and another resistor in series with them to reduce baseline drift. He also eliminated the problem arising from temperature and voltage controls, and consequently achieved a better detection limit.

Above the self-heating point, thermistors have a negative incremental resistance. This may give rise to a negative output impedance of a Wheatstone bridge, with potentially very high gain under loaded conditions. Attendant time constants make this impractical<sup>34</sup>. The Du Pont-ERL bridge<sup>30,33</sup> was developed to null out power supply noise by matching noise sensitivities. This is done by unbalancing the currents in the two legs in such a way that the response of two thermistors to power supply noise are equal. The same approach can be used for temperature variations. The advantage of the Du Pont-ERL bridge is in that it nulls out either the noise arising from the current or the temperature. Buhl<sup>34</sup> uses the Du Pont-ERL technique to attain a temperature null and adds resistors in parallel with the sensing elements to achieve current nulling. With this, the bridge would always have a non-zero output which can be remedied by a dc offset system, although with sub microvolt output signals, stability may be hard to achieve.

Madden et al.<sup>35</sup> observed that a thermal conductivity bridge powered by ac produced a poor resistive balance. With 50-cycle ac power, they obtained a good residual balance potential. By placing a Twin-T filter tuned to 150 Hz in the amplifier circuit, they removed the 2nd harmonic signal and thereby improved the null point of the thermal conductivity bridge.

Attempts have been made by a few investigators to amplify the dc output



of the thermal conductivity bridge<sup>36,37</sup>. Burg et al.<sup>37</sup> placed a manganin resistor across the amplifier to reduce the input impedance. Bennet et al.<sup>36</sup> did not have a feedback circuit on their amplifier, so that amplification varied as the attenuation of the bridge changed. They reported the effective full scale to be between 40-1000  $\mu\text{V}$ , but chose a 25  $\mu\text{V}$  range for the experimental work. The noise level at the bridge was given as 0.1-0.2  $\mu\text{V}$ . A drift of about 5.0-10.0  $\mu\text{V}$  was noted. Fluctuations at the thermistors were the primary reason for the drift. The amplifier was linear at signals less than 300  $\mu\text{V}$ .

In view of the complications and sensitive instrumentation required when dc operated thermal conductivity detectors are used, Furst et al.<sup>38</sup> employed an ac current produced by a 1000 Hz vacuum tube oscillator to operate the katharometer. The current was amplified by a second tube and coupled to the bridge by a center-tapped transformer to give a push-pull drive. The authors indicate a variation of sensitivity through gain control and also the possibility for logarithmic response through use of remote cut-off tubes, indicating that their amplifier was probably open-loop, so that they must count on gain stability. The bridge output was rectified without phase discrimination, i.e. bridge unbalance in both directions would give a positive dc output. There is no claim for increased sensitivity.

Kieselbach<sup>30</sup> studied the various sources of noise in thermistor detectors and verified that the principal contributors were external to the thermistor. These are bridge-current, flow, ambient temperature variations, shock and vibration. The author eliminated leakage to ground in the wiring by bringing the common mode of the detector bridge output to ground

potential; mismatch of the resistances of the thermistors was decreased by operation at the same temperature rather than at the same current. Kieselbach improved stability at the expense of a small loss in sensitivity by having higher resistance loads which minimized the effects of stray resistance and thermal emfs in cables and connectors between the detector and the remainder of the bridge circuit. The noise arising from the servo amplifier was negligible when compared to that of the main noise. Through his modifications, he achieved a 50-fold improvement in the S/N (signal to noise) ratio over the conventional design.


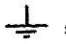
Papers by Grice and Winefordner, though not related to thermal conductivity detectors should be mentioned here. Grice et al.<sup>39</sup> describe an ultrasonic cell which is capable of detecting 0.5 ppm H<sub>2</sub> in argon. This is comparable to the performance of our system. The cell in its present form is limited to temperatures of 200°C; furthermore, the system is not compatible with the thermal conductivity blocks which are a part of the vast majority of gas chromatographs in use today. Winefordner et al.<sup>40</sup> describe detectors which are based on the dielectric properties of gas mixtures which may be monitored either by frequency of an RF oscillator, or by the RF field distribution in a capacitor containing the sample gas. Detection limits vary from 2-8 ppm for most gases. The dynamic range was reported as 10<sup>2</sup> to 10<sup>4</sup>.

#### CONSTRUCTION:

Nearly all of the components of our solid-state instrument are mounted on 4" x 4" copper-plated circuit boards. First the circuit lay-out is drawn on a 4" x 4" paper which is pasted to the board. Holes corresponding to the location of the component leads are drilled with 3/64-inch drill bit. The portion of the board that fits into the socket is inserted into the socket so that metal contacts in the female part make traces on the copper to assure proper location of edge contacts. The boards are cleaned with acetone, marked with a resist marking pen (RMP-700), and etched in a warm solution (20%, w/w) of ammonium persulfate. Then the boards are rinsed with water and acetone respectively to reveal the design. The components are soldered. The foil side of the boards except the edge contacts are sprayed with "clear acrylic spray" to prevent air oxidation of copper. The circuit boards are inserted into 15-pin socket connectors which in turn are fastened to an aluminum chassis, to provide connections between different socket pins.

Commercial and home-made heat dissipators are used on transistors where large amounts of heat are produced. The size of a heat dissipator depends upon ambient temperature and the maximum average power that the transistor dissipates. Transistors on the same board having a common collector connection may be inserted into a single aluminum heat dissipator. Those transistors which do not have a common collector connection obviously must have separate heat sinks.

In circuits where low level signals are handled, special attention must be given to system grounding. There is always a certain amount of potential drop between multiple grounds in a single circuit resulting from inductive

and/or capacitive coupling between the presumably isolated circuits. This may result in sufficient cross-talk to mask the millivolt or low level signal. To avoid this, our system has a signal ground, , and a power ground, , which are independently connected to one central point on the chassis. Signal ground is connected at only one point, and signal cable shields are connected to the signal ground. All other cable shields are connected to power ground<sup>41,42</sup>.

## SYMBOLS:

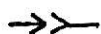
R	Resistor
C	Capacitor
D	Diode
Q	Transistor
P	Potentiometer, ganged or trim.
L	Pilot light
T	Transformer
S	Switch
F	Fuse



Power ground



Signal ground



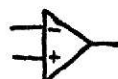
Socket pin connection



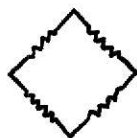
Jumper



Booster



Operational amplifier



Wheatstone bridge

#### ELECTRONIC CIRCUITS:

The six boards contain a regulated power supply, smoothed high current supply, oscillator and clamps, common mode rejection amplifier and current boosters, preamplifier and demodulator, and dc-ac switching circuit.

Trim potentiometers,  $P_1$  and  $P_2$ , for initial adjustments are located on the regulated power supply board. All operating controls (potentiometers for vertical and horizontal symmetry, ganged potentiometers for frequency and amplitude adjustment of the square-wave, potentiometers for the fine and coarse adjustments of the thermal conductivity bridge, attenuator for the output signal, pilot lamps, and switches) are mounted on the front panel of the instrument. A fuse and shielded connectors for supply, input and recorder are mounted on the back of the panel. Transformers are mounted directly on the chassis. The circuits will be discussed in the order given above.

### The Regulated Power Supply: Fig. 5

The regulated power supply is electrically symmetrical with respect to ground. The top half will be discussed first and then the variations in the bottom half will be explained.

A rectifier,  $D_1$ , and storage capacitor,  $C_1$ , form the heart of the power supply. Resistor  $R_3$  provides a short circuit protection for the transistor pair  $Q_1$  and  $Q_2$ . Capacitor  $C_2$  along with resistors  $R_1$  and  $R_2$  act as a filter for the base current of transistor  $Q_2$ <sup>43</sup>. The transistor reference amplifier RA1 amplifies the error signal developed between the reference voltage at the emitter of this transistor and a fraction of the positive output determined by potentiometer  $P_1$ . The amplified error signal forms the input to pass transistor  $Q_2$  via Darlington transistor  $Q_1$  which decreases output impedance<sup>44</sup>. Capacitor  $C_3$  improves high frequency stability. To allow remote sensing of the output voltage, the top lead of  $R_4$  is brought out to a connector pin. Diode  $D_2$  serves to prevent the output from going high in the event of an open circuit in the sensing lead.

The bottom half is based on a similar circuit, but to insure symmetry, the positive regulated output serves as a reference voltage for the negative supply. A transistor pair,  $Q_3$  and  $Q_4$ , rather than single transistor with grounded emitter, is used as comparison amplifier, to improve thermal tracking of the 2 outputs.

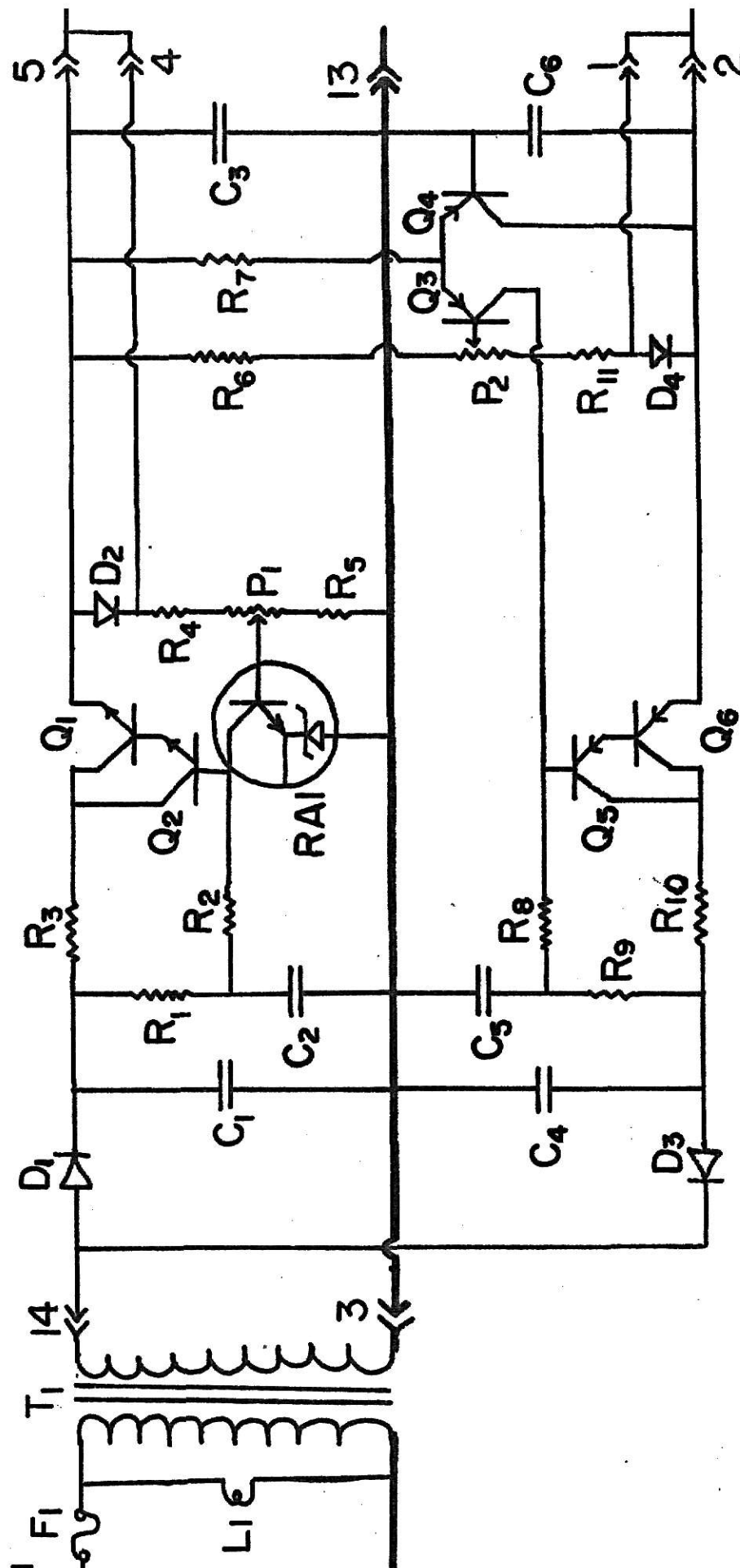
Remote sensing eliminates stray output impedance due to connector resistance. Two separate contacts at pin connections, 3 and 13, are provided for current paths for ac return and dc ground to prevent ac pick-up.

The values of the components are chosen to provide +15 and -15 volts regulated at approximately 100 mA. The voltages are adjusted to the

nearest 0.01 volt with the two trim potentiometers,  $P_1$  and  $P_2$ .



# BOARD I REGULATED POWER SUPPLY



**Fig. 5**

The Smoothed High Current Supply: Fig. 6

The circuit produces +14 and -14 volts filtered at up to 400 mA. The bases of the transistors, Q<sub>7</sub> and Q<sub>8</sub>, are powered by +15 and -15 volts respectively. The resistors act as protective elements for the transistors.

# BOARD II

## SMOOTHED HIGH CURRENT SUPPLY

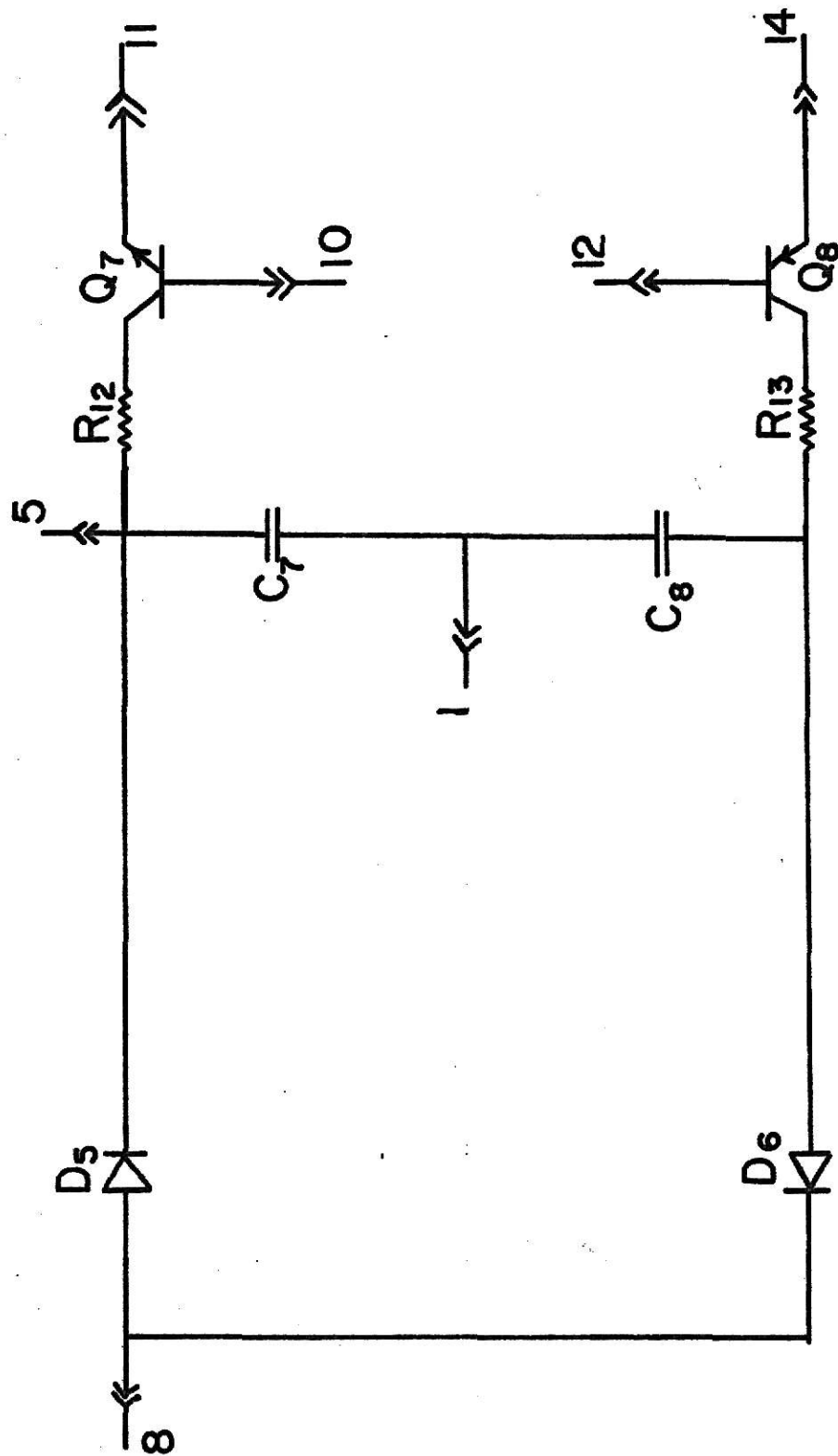


Fig.6

### The Oscillator and the Clamps: Fig. 7

#### The Oscillator:

This is essentially a multivibrator. Base of transistor  $Q_{10} \longrightarrow$  collector of transistor  $Q_{10} \longrightarrow$  base of transistor  $Q_{11} \longrightarrow$  collector of transistor  $Q_{11} \longrightarrow$  base of transistor  $Q_{10}$  constitute the regenerative loop. As soon as the circuit is turned on, the system enters a state in which one transistor is conducting while the other one is cut off<sup>45</sup>. Transistors  $Q_9$  and  $Q_{12}$  ensure quicker charging of capacitors  $C_9$  and  $C_{10}$  respectively<sup>46</sup>. Consequently, the square-wave produced has sharp rising edges. Diodes  $D_7$  and  $D_8$  provide a pathway for the discharging of capacitors  $C_9$  and  $C_{10}$  respectively.

The outputs to the clamps and to the field effect transistors,  $Q_{21}$  and  $Q_{22}$  in Fig. 10, are taken from low impedance points at the emitters of transistors  $Q_9$  and  $Q_{12}$  as shown in the circuit. Diodes  $D_9$ ,  $D_{10}$ , resistors  $R_{21}$ ,  $R_{22}$ , capacitor  $C_{17}$  and diodes  $D_{11}$ ,  $D_{12}$ , resistors  $R_{24}$ ,  $R_{25}$ , capacitor  $C_{18}$  produce delayed gate signals for the demodulator switches.

The frequency of the square-wave of the oscillator depends on the product of  $C_9$  and  $P_5$ , and  $C_{10}$  and  $P_3$ .  $P_5$  and  $P_3$  are mounted on a common shaft.  $P_4$  allows fine adjustment of horizontal symmetry. The oscillator produces a square-wave in the frequency range 160-1000 cycles per second.

#### The Clamps:

The clamps are electrically symmetrical with respect to ground. The negative and the positive voltages of the square-wave are clamped with the top half and the bottom half respectively. The magnitude of the square-wave can be varied from 4-20 volts p-p; the clamped voltages are referred to regulated  $\pm 15$  volts.

The negative clamp will be discussed here only. This is basically a voltage regulator with its feedback loop as shown in Fig. 8.

# BOARD III OSCILLATOR AND CLAMPS

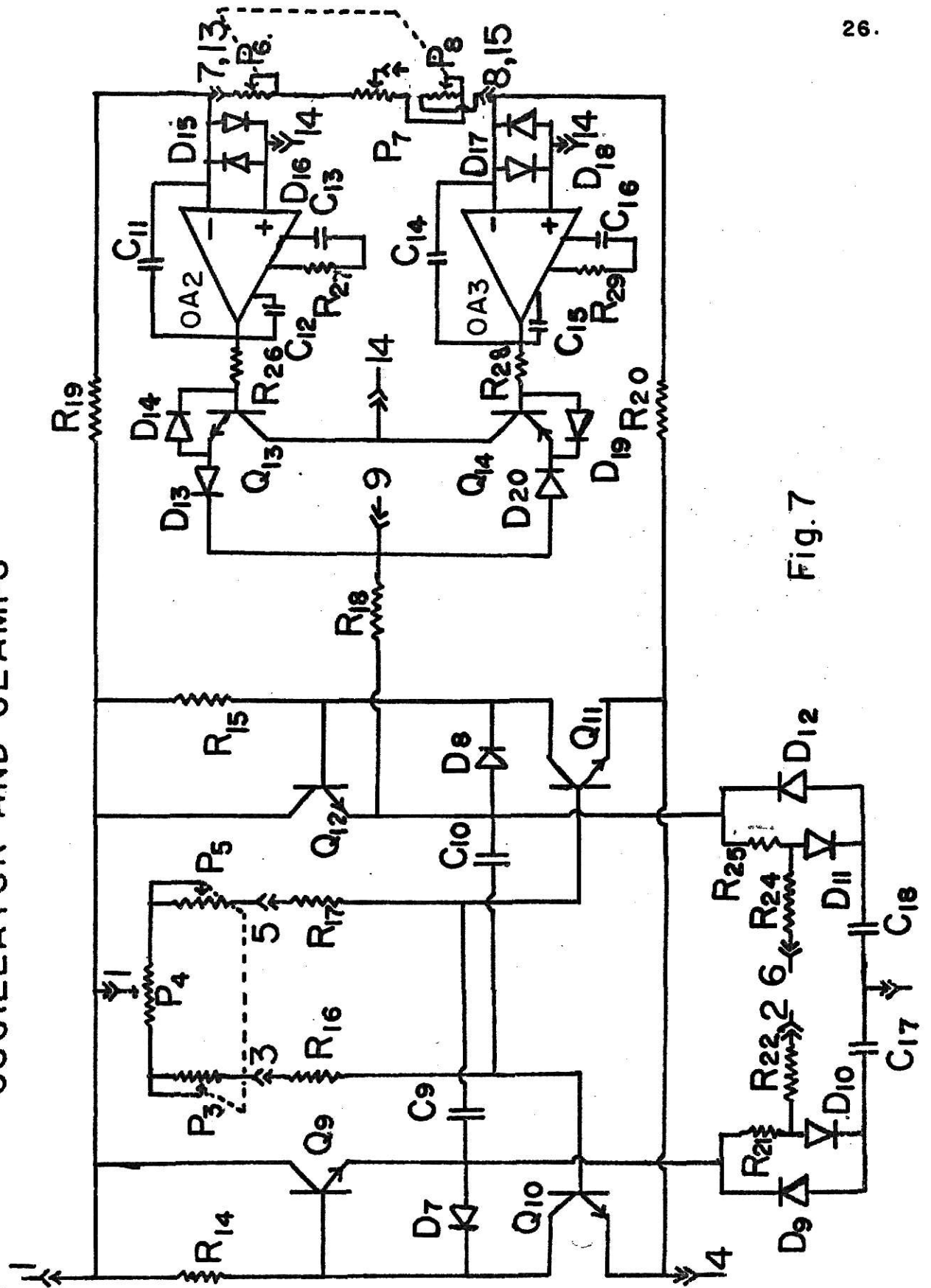


Fig. 7

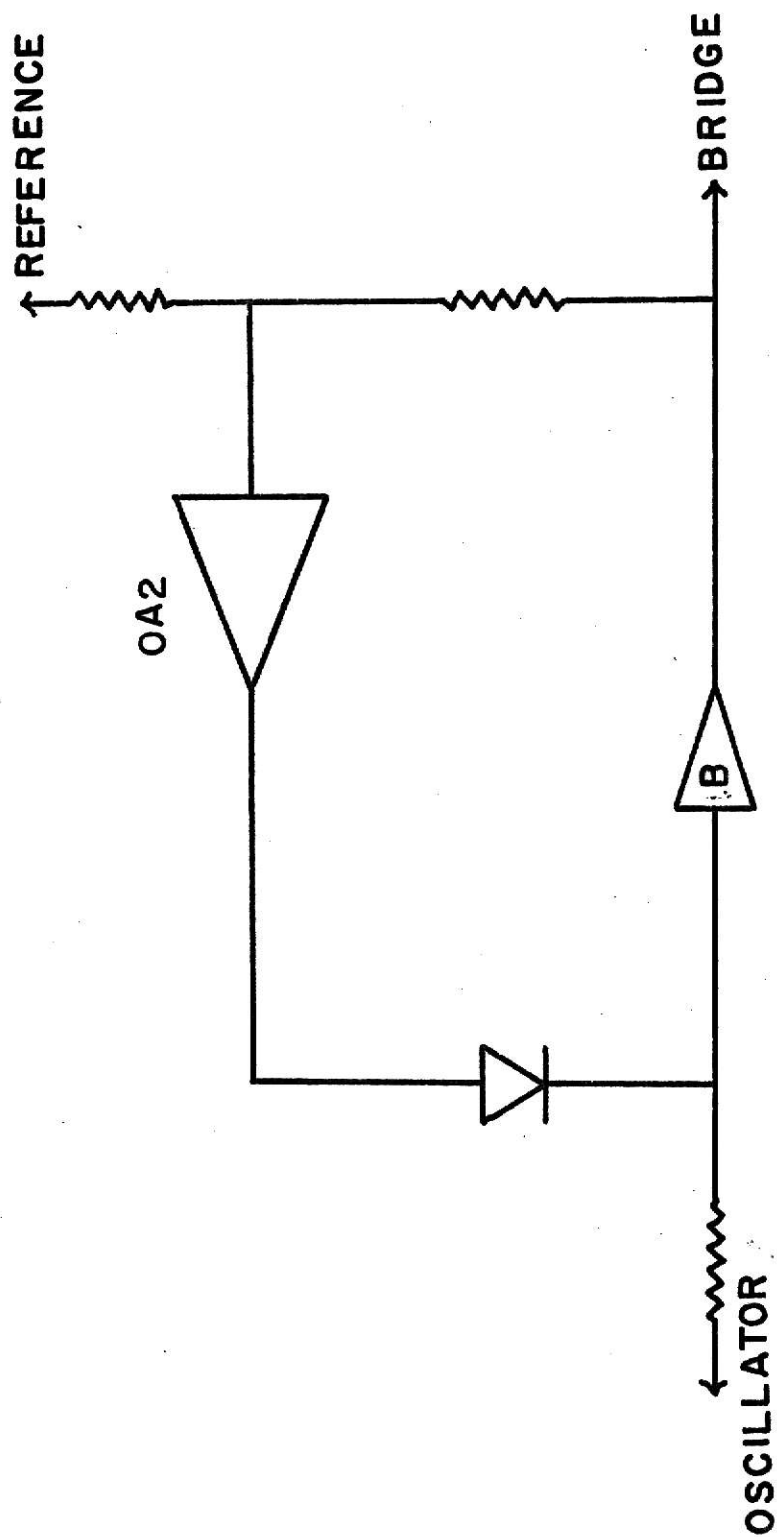


Fig.8

Diode  $D_{13}$  opens the feedback loop for negative output of the  $\mu A709C$  amplifier, i.e. for positive bridge voltage. Transistor  $Q_{13}$  is added to provide current amplification. The output stage of the operational amplifier is protected against excessive current by resistor  $R_{26}$ ; diode  $D_{14}$  serves to protect transistor  $Q_{13}$  against excessive reverse base voltage. Diodes  $D_{15}$  and  $D_{16}$  protect the inverting input of the operational amplifier  $\mu A709C$  against excessive input voltages. Capacitor  $C_{11}$  was added between the inverting input and output of  $\mu A709C$  to prevent oscillation. Furthermore, the operational amplifier was compensated with capacitors  $C_{12}$ ,  $C_{13}$  and resistor  $R_{27}$  as recommended by the manufacturer. With the components shown, the gain of the amplifier is  $10^3$  at 10 kHz and  $10^4$  at 1 kHz<sup>47</sup>.



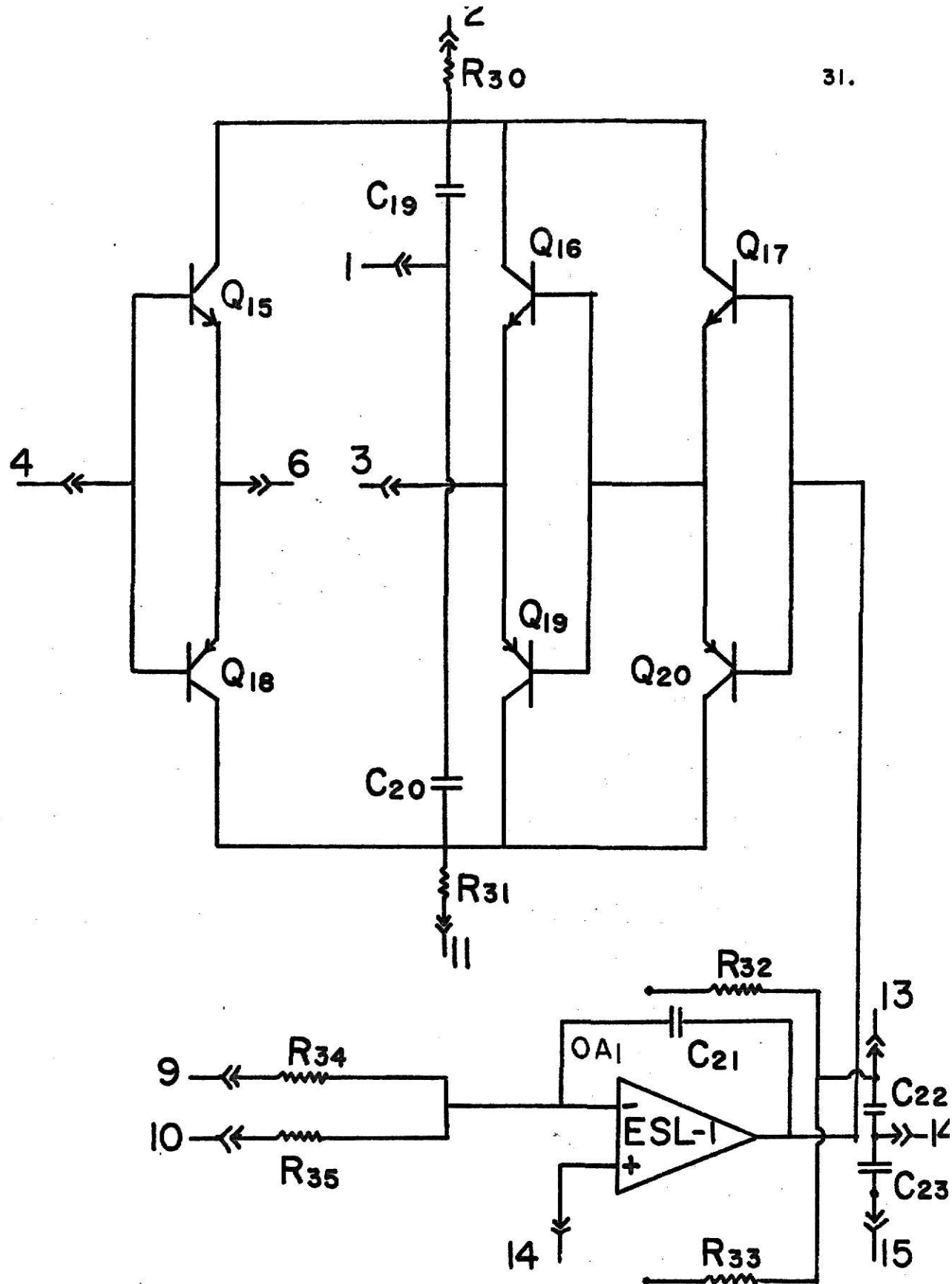
### Common Mode Rejection Drive and Current Boosters: Fig. 9

The  $\pm 14$  filtered voltage is used to provide the high current through the bridge. Transistor pairs  $Q_{15}$  and  $Q_{18}$ ,  $Q_{16}$  and  $Q_{19}$ ,  $Q_{17}$  and  $Q_{20}$  supply the bridge with high current square-wave power. The magnitude of the voltages of the square-wave at the bridge inputs 6 and 3 are equal but there is a phase difference of  $180^\circ$ . Filters  $C_{19}$ ,  $R_{30}$  and  $C_{20}$ ,  $R_{31}$  were added to prevent radiation of switching noise.

The operational amplifier OA 1 holds the average of the bridge output, 9 and 10, at ground potential. Capacitor  $C_{21}$  prevents the operational amplifier from oscillating. Capacitors  $C_{22}$  and  $C_{23}$  minimize the radiation of noise. Resistors  $R_{34}$  and  $R_{35}$  are matched resistors. Resistors  $R_{32}$  and  $R_{33}$  are connected to the amplifier offset terminals as recommended by the manufacturer.

The square-wave at the input of the bridge has sharp spikes on it due to the finite response speed of the clamping and common mode rejection. These spikes also appear on the output unbalance of the bridge, but are eliminated at the demodulator as will be discussed later.

Figure 9. Circuit diagram for current boosters and common mode rejection amplifier.



# CURRENT BOOSTERS AND COMMON MODE REJECTION DRIVE BOARD IV

### Preamplifier, Demodulator and Attenuator: Fig. 10

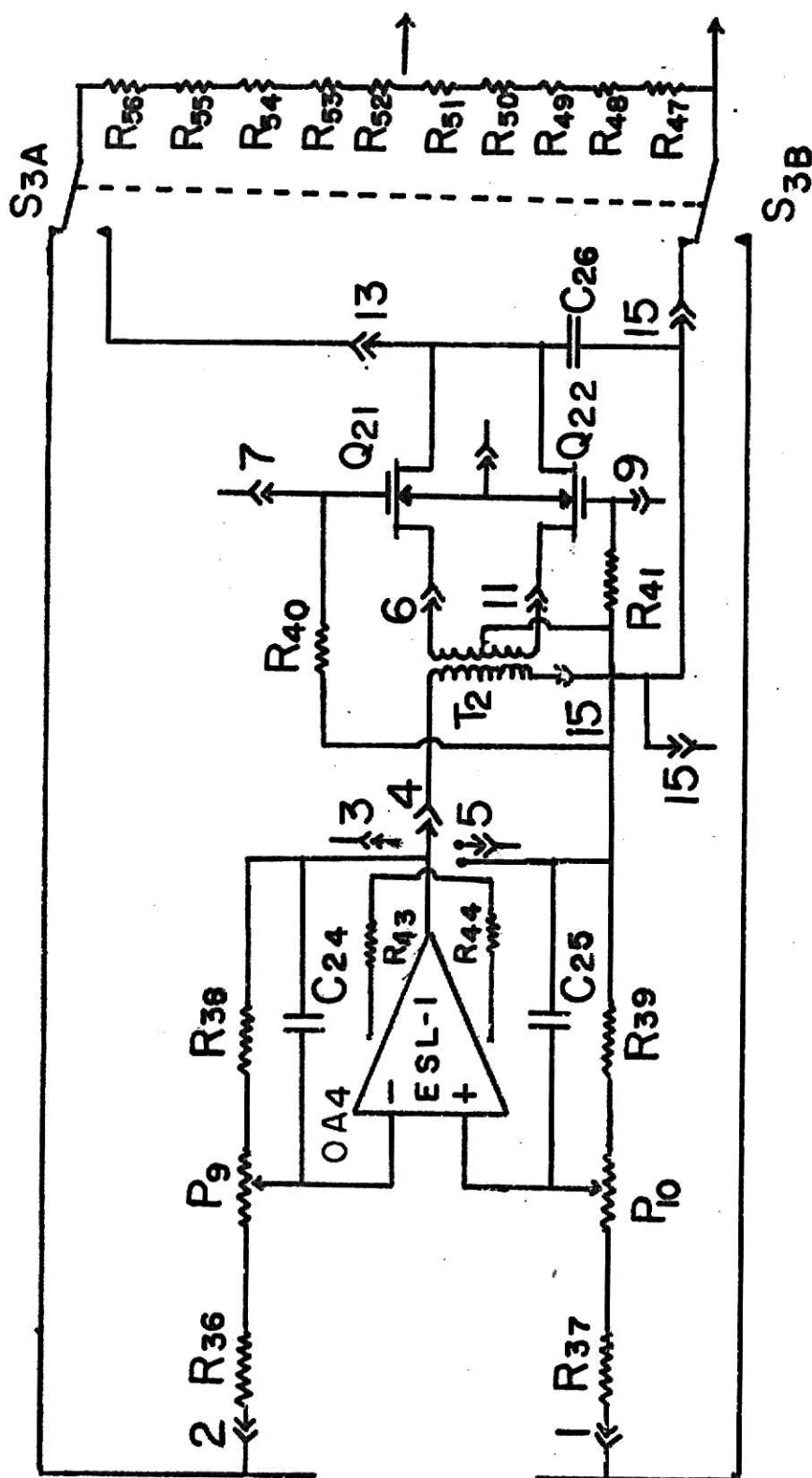
The bridge output, 1 and 2, consists of two complementary square-wave signals. The operational amplifier OA 4 is connected as a difference amplifier. It algebraically subtracts the two complementary square-wave signals and amplifies the difference with a gain of 100. Capacitor  $C_{24}$  was placed between the inverting input and the output of the amplifier to prevent oscillation; capacitor  $C_{25}$  maintains symmetry. The ratios of  $R_{38}/R_{36}$  and  $R_{39}/R_{37}$  which determine the gain are made equal to approximately 100 through the adjustment of  $P_9$  and  $P_{10}$  respectively. The addition of resistors  $R_{43}$  and  $R_{44}$  is recommended by the manufacturer for offset nulling of OA 4.

The amplified square-wave signal is changed into two square-wave signals that are  $180^\circ$  out of phase by a 1:2 transformer with a center tap on the secondary. This transformer also blocks any unwanted dc voltages. Each of the square-wave signals is fed to the MOS-FET's. The gates of the MOS-FET's are controlled by a square-wave with delayed rise times from the oscillator at 7 and 9. Gate voltages are +6 volts and -4 volts with respect to ground potential. The magnitude of the positive and negative voltages depends on the values of the resistors  $R_{21}$ ,  $R_{22}$ ,  $R_{40}$  and  $R_{24}$ ,  $R_{25}$ ,  $R_{41}$ .  $R_{40}$  and  $R_{41}$  between the gates, 7 and 9, respectively, and ground potential protects the gate insulation against static charge when the circuit is removed from its socket.

When the gate-to-source voltage is approximately -4 volts, drain-to-source impedance is about 1000 megaohms, while at voltages higher than -1 volt, the drain-to-source impedance is less than 1 Kohms<sup>48</sup>. The function of the two FET's is comparable to full wave rectification. This rectification

produces a dc signal whose magnitude is directly proportional to the bridge unbalance, which in turn is directly proportional to the concentration of the sample component at the detector filament.

The gain of the overall system is reduced to 85 due to the wave-form applied at the gates of the FET's. This 15% loss of the signal eliminates the sharp spikes on the square-wave of the transformer output which otherwise would have contributed to noise of the overall system.



BOARD V  
PREAMPLIFIER, DEMODULATOR AND ATTENUATOR

Fig. 10

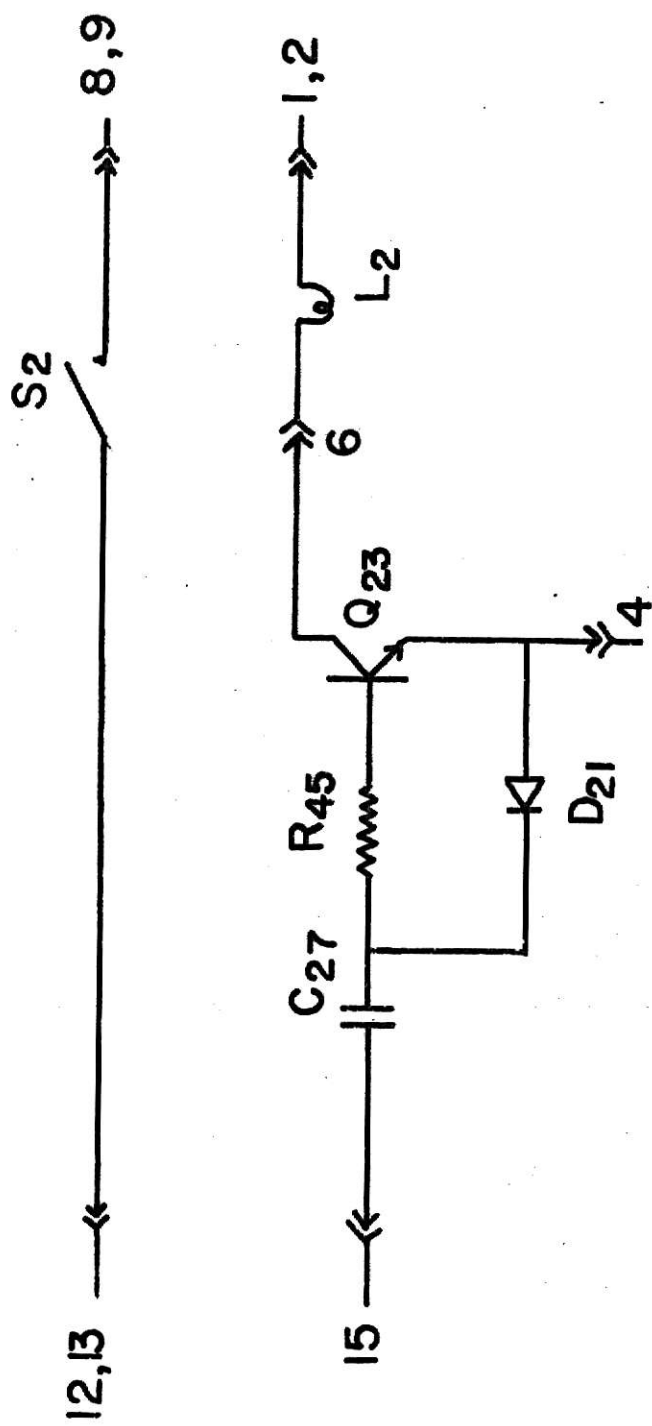
Dc-ac Switching System: Fig. 11

The purpose of introducing this circuit into the oscillator circuit is two-fold;

1. To start the oscillator after initial application of power.

Shorting the emitter and base of transistor  $Q_{10}$  with the switch primes the system for oscillation. When the switch is then opened, the oscillator will start reliably. When the switch is opened, the output is coupled by capacitor  $C_{27}$  to transistor  $Q_{23}$ , which rectifies and amplifies the ac signal and drives indicator light  $L_2$ .

2. To provide dc power to the bridge. When the switch  $S_2$  is closed, the emitter to base of  $Q_{10}$  is shorted and the oscillator is paralyzed. Under these conditions the bridge is supplied with dc power under control of clamping amplifier  $\mu A709C$ ; therefore, exactly equal ac and dc power levels are available for comparison purposes.



BOARD VI

AC-DC SWITCHING CIRCUIT

Fig. II



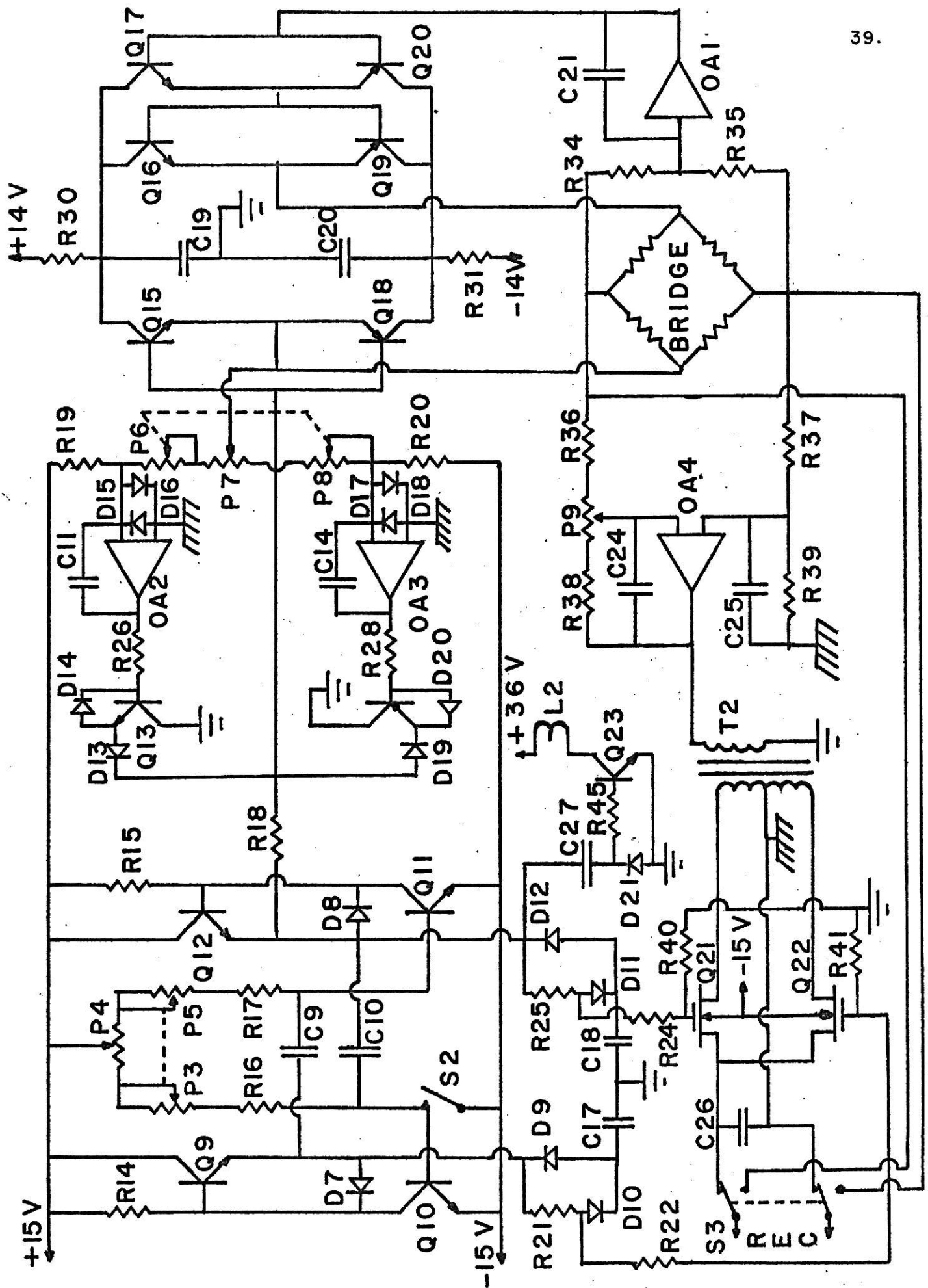
### Complete Circuit: Fig. 12

Complete circuit entails the oscillator and the clamps, Fig. 7, current boosters and common mode rejection amplifier, Fig. 9, preamplifier, demodulator and part of the attenuator, Fig. 10, and dc-ac switching circuit, Fig. 11.

Socket pin connection numerals are intentionally omitted. Instead,  $\pm 15$  volt dc and  $\pm 14$  volt dc supply, signal and power ground symbols are directly indicated to give more meaning to the viewer.

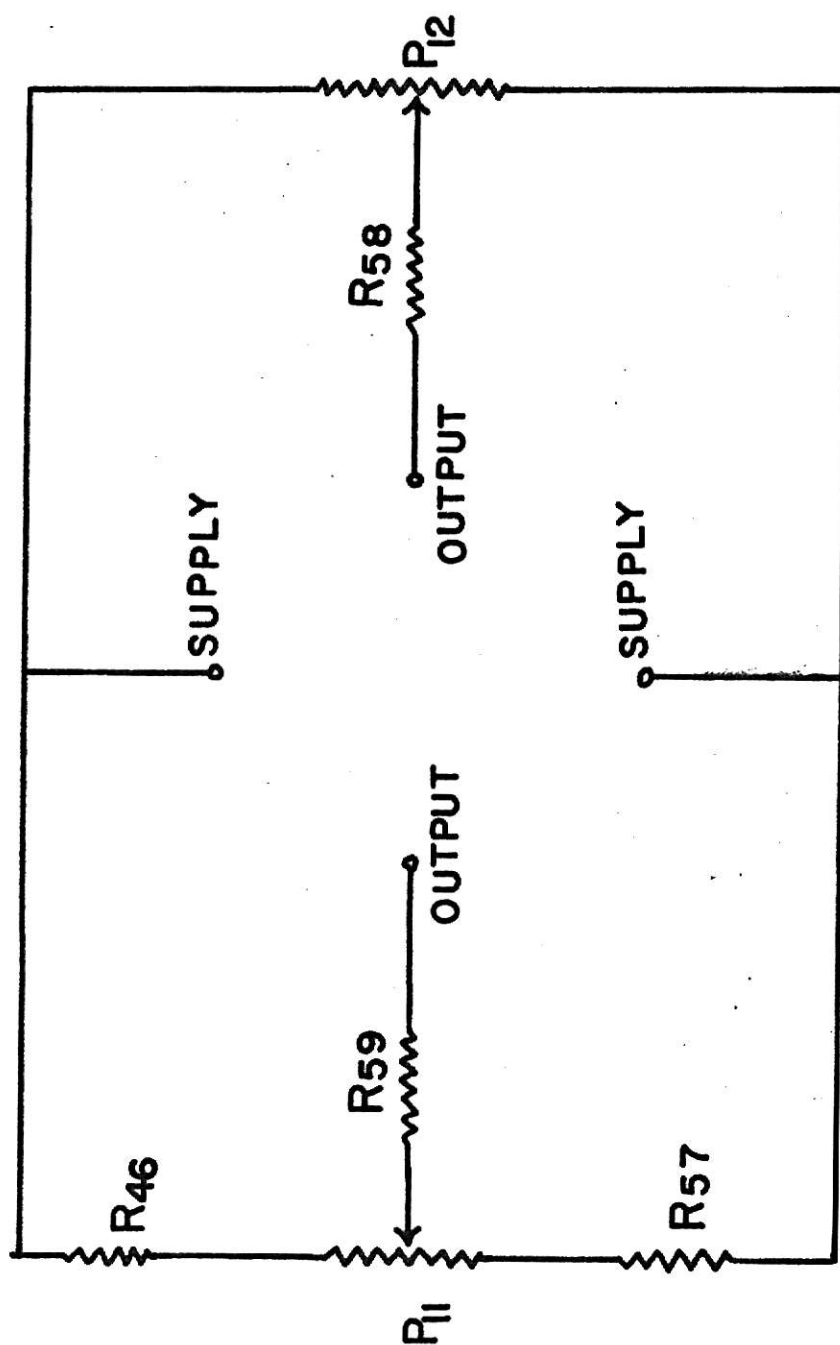
The internal compensating and/or nulling components of the operational amplifiers are also neglected because of the limit on space.

Figure 12. Complete circuit. It contains oscillator and clamps, common mode rejection amplifier and current boosters, preamplifier and demodulator, and dc-ac switching circuits.



Bridge Control Circuit: Fig. 13

The components of this circuit are located on the back of the front panel. Trim potentiometer  $P_{12}$  and resistor  $R_{58}$  serve as a coarse control while 3-turn potentiometer  $P_{11}$  and resistors  $R_{46}$ ,  $R_{57}$ ,  $R_{59}$  serve as a fine control in zeroing the bridge output.

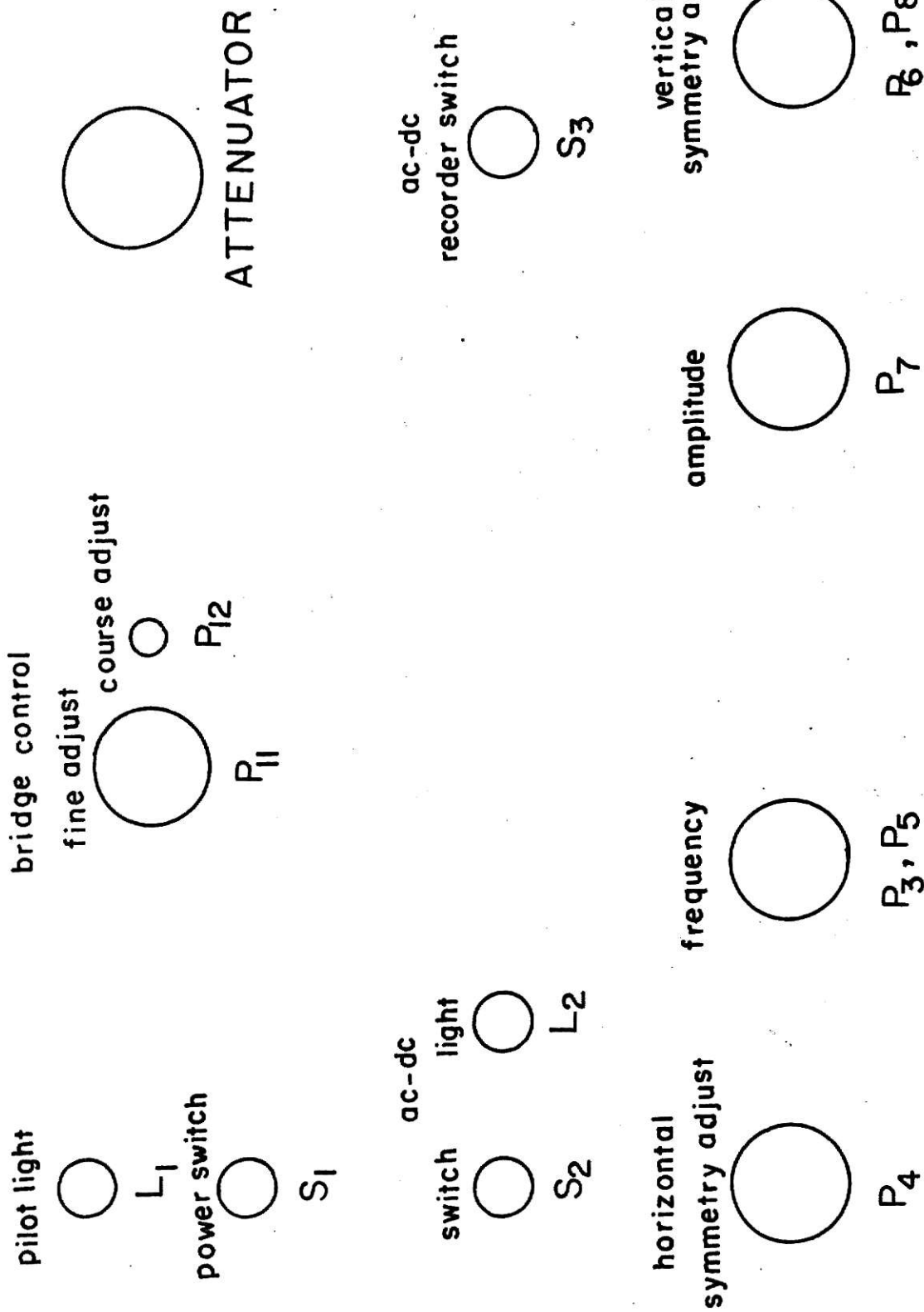


BRIDGE CONTROL CIRCUIT

Fig.13

Front Panel: Fig. 14

The schematic diagram indicates the location of the externally adjustable components of the instrument.



FRONT PANEL OF THE INSTRUMENT

Fig. 14

## Regulated Power Supply: (Fig. 15) Board I

## Socket pin connections:

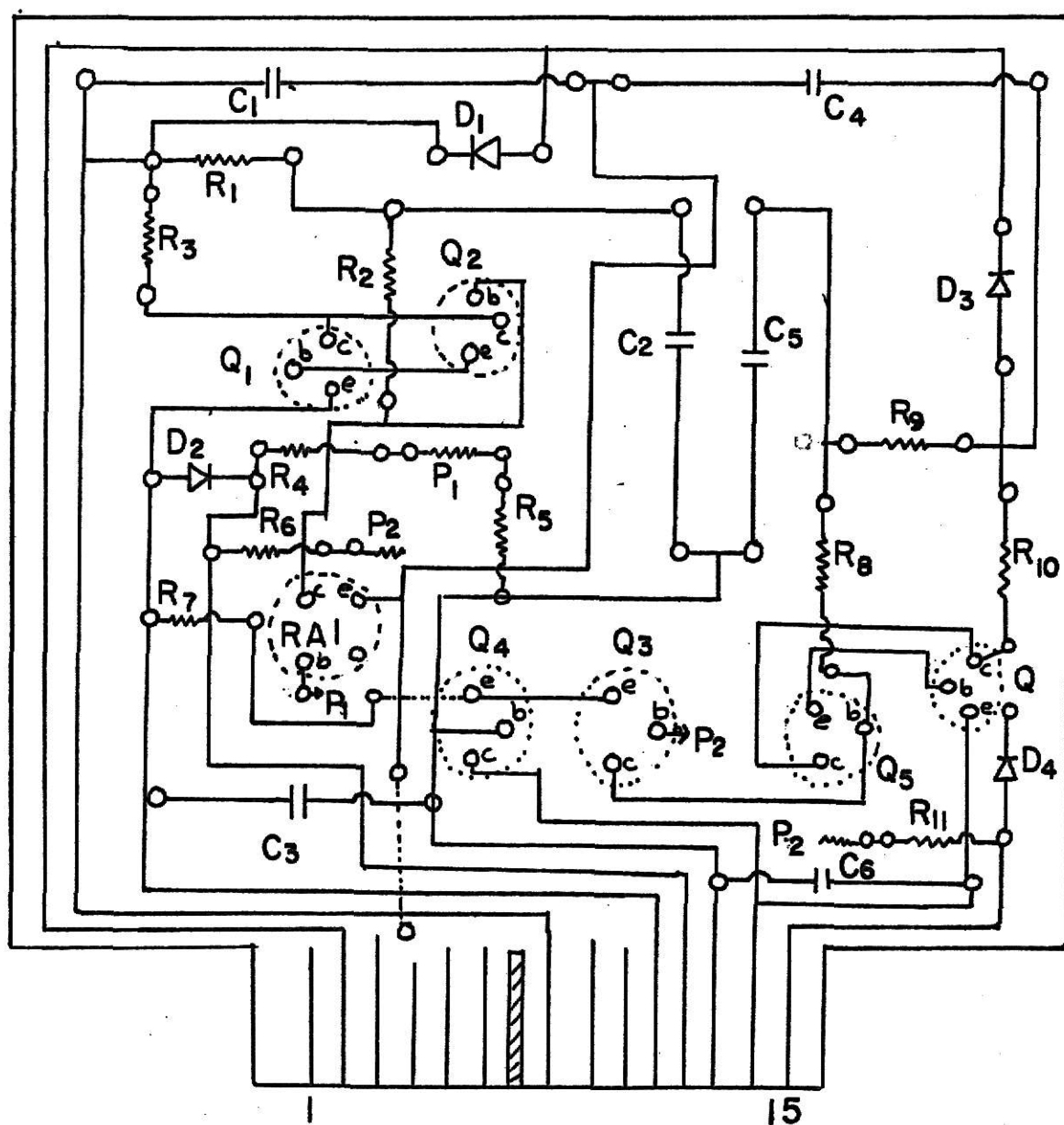
1	-15 volt dc output
2	-15 volt dc remote sense
3	ac ground
4	+15 volt dc out
5	+15 volt dc remote sense
6	N. C.
7	key
8	N. C.
9	N. C.
10	N. C.
11	N. C.
12	N. C.
13	dc ground
14	ac power in
15	N. C.



## Regulated Power Supply: (Fig. 15) Board I

## Parts List:

C <sub>1</sub> , C <sub>4</sub>	500 $\mu$ F/50v
C <sub>2</sub> , C <sub>3</sub>	100 $\mu$ F/50v
C <sub>5</sub> , C <sub>6</sub>	25 $\mu$ F/25v
D <sub>1</sub> , D <sub>3</sub>	1N3253
D <sub>2</sub> , D <sub>4</sub>	1N34
F <sub>1</sub>	fuse, 1/2 amp.
L <sub>1</sub>	pilot light
P <sub>1</sub> , P <sub>2</sub>	700 ohm trim potentiometer
Q <sub>1</sub>	2N1613
Q <sub>2</sub>	2N3417
Q <sub>3</sub> , Q <sub>4</sub> , Q <sub>5</sub>	2N508A
Q <sub>6</sub>	2N4037
RA1	RA1
R <sub>1</sub> , R <sub>2</sub> , R <sub>9</sub>	4.7K
R <sub>3</sub> , R <sub>10</sub>	150 ohm
R <sub>4</sub> , R <sub>5</sub>	820 ohm
R <sub>6</sub> , R <sub>11</sub>	1.5K
R <sub>7</sub>	3.9K
R <sub>8</sub>	10K
S <sub>1</sub>	SPDT
T <sub>1</sub>	25-volt, 1 amp
Heat sinks, separate: Q <sub>1</sub> , Q <sub>6</sub>	



ETCH PATTERN BOARD I, FOIL SIDE

**Fig. 15**

Smoothed High Current Supply: (Fig. 16) Board II

Parts List:

C <sub>7</sub> , C <sub>8</sub>	1000 $\mu$ F/50v
D <sub>5</sub> , D <sub>6</sub>	1N3253
Q <sub>7</sub>	2N3053
Q <sub>8</sub>	40394
R <sub>12</sub> , R <sub>13</sub>	25 ohm 5w

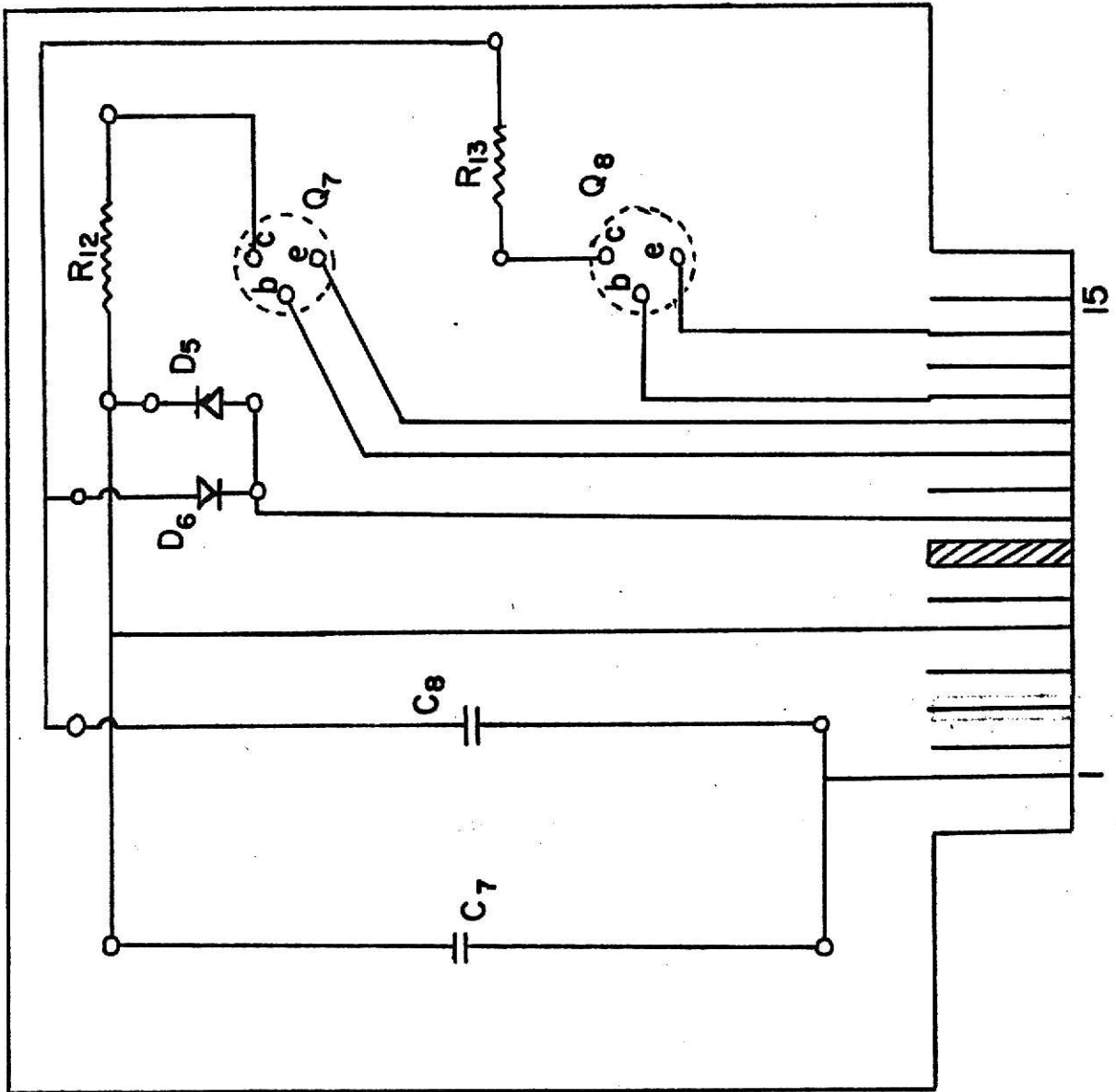
Heat sinks, separate; Q<sub>7</sub>, Q<sub>8</sub>

## Smoothed High Current Supply: (Fig. 16) Board II

## Socket pin connections:

1	power ground
2	N. C.
3	N. C.
4	N. C.
5	+36 volt dc
6	N. C.
7	key
8	ac in
9	N. C.
10	+15 volt dc in
11	+14 volt dc in
12	-15 volt dc in
13	N. C.
14	-14 volt dc out
15	N. C.

Figure 16. The arrangement of components of Board II as viewed from the foil side.



ETCH PATTERN BOARD II, FOIL SIDE

## Oscillator and Clamps: (Fig. 17) Board III

## Parts List:

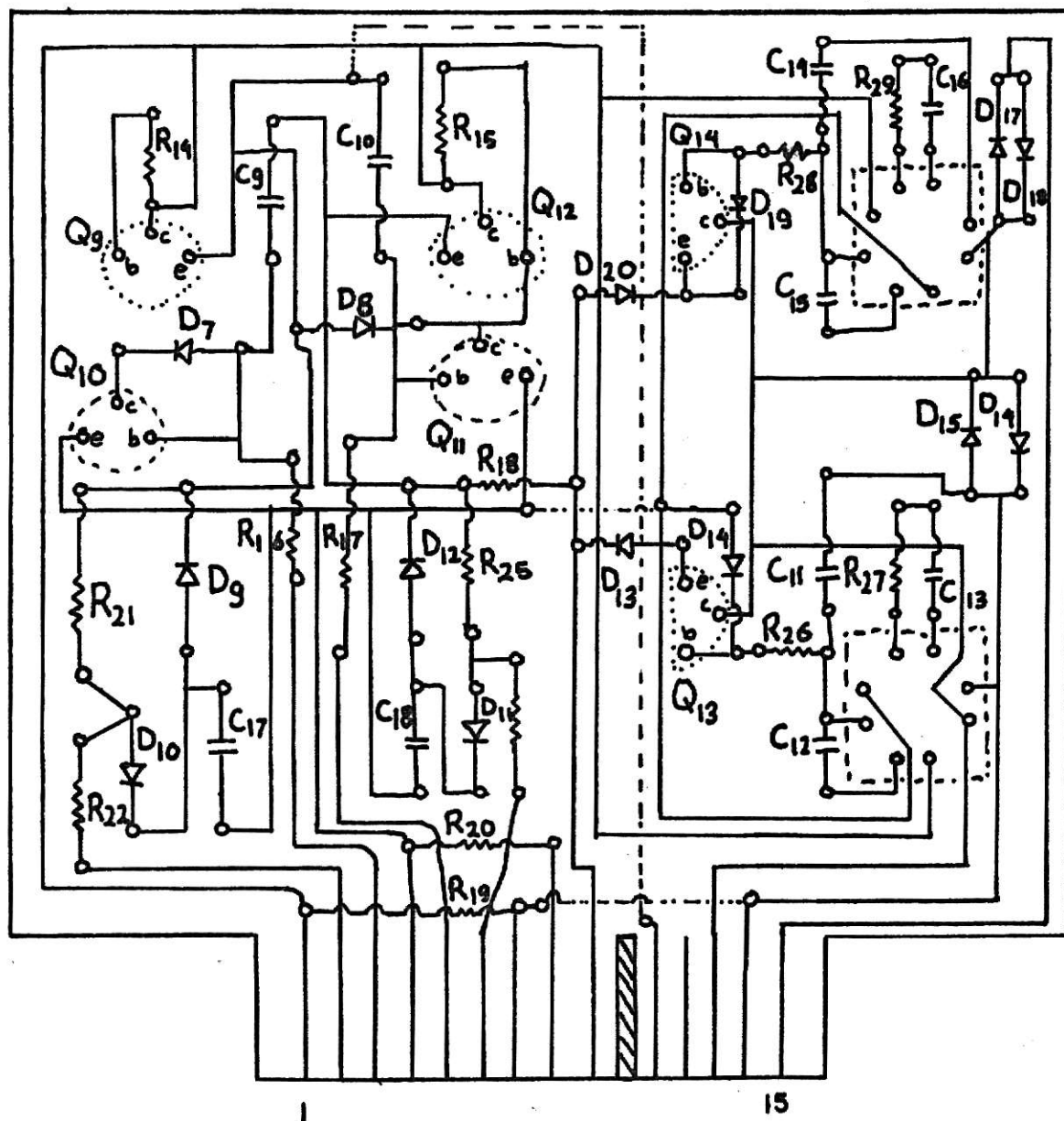
C <sub>9</sub> , C <sub>10</sub>	.047 $\mu$ F
C <sub>11</sub> , C <sub>14</sub>	100 $\mu$ F
C <sub>12</sub> , C <sub>15</sub>	20pF
C <sub>13</sub> , C <sub>16</sub>	470pF
C <sub>17</sub> , C <sub>18</sub>	.001 $\mu$ F
D <sub>7</sub> , D <sub>8</sub> , D <sub>9</sub> , D <sub>10</sub>	1N914
D <sub>11</sub> , D <sub>12</sub> , D <sub>13</sub>	1N914
D <sub>14</sub> , D <sub>15</sub> , D <sub>16</sub>	1N34
D <sub>17</sub> , D <sub>18</sub> , D <sub>19</sub>	1N34
D <sub>20</sub>	1N914
P <sub>3</sub> , P <sub>5</sub>	250K ganged potentiometer
P <sub>4</sub>	50K
P <sub>6</sub> , P <sub>8</sub>	10K ganged potentiometer
P <sub>7</sub>	1K
Q <sub>9</sub> , Q <sub>10</sub> , Q <sub>11</sub> , Q <sub>12</sub> , Q <sub>13</sub>	2N3417
Q <sub>14</sub>	2N2953
R <sub>14</sub> , R <sub>15</sub>	12K
R <sub>16</sub> , R <sub>17</sub>	10K
R <sub>18</sub>	560 ohm
R <sub>19</sub> , R <sub>20</sub>	5.6K
R <sub>21</sub> , R <sub>25</sub>	270K
R <sub>22</sub> , R <sub>24</sub>	150K
R <sub>26</sub> , R <sub>28</sub>	1K
R <sub>27</sub> , R <sub>29</sub>	1.5K
OA2, OA3	Fairchild $\mu$ A709C

## Oscillator and Clamps: (Fig. 17) Board III

## Socket pin connections:

1	+15 volt dc
2	gate of $Q_{21}$
3	CW of $P_3$
4	-15 volt dc
5	CW of $P_5$
6	gate of $Q_{22}$
7	CW of $P_6$
8	CW of $P_8$
9	bridge drive
10	key
11	dc-ac switching system
12	N. C.
13	same as 7
14	signal ground
15	same as 8





ETCH PATTERN BOARD III, FOIL SIDE

Fig. 17

## Current Boosters and Common Mode Rejection Amplifier: (Fig. 18) Board IV

## Parts List:

C <sub>19</sub> , C <sub>20</sub>	2.5 $\mu$ F
C <sub>21</sub>	56pF
C <sub>22</sub> , C <sub>23</sub>	.047 $\mu$ F
Q <sub>15</sub> , Q <sub>16</sub>	2N1613
Q <sub>17</sub>	2N1711
Q <sub>18</sub> , Q <sub>19</sub>	40394
Q <sub>20</sub>	2N2953
R <sub>30</sub> , R <sub>31</sub>	15 ohm 4w
R <sub>32</sub> , R <sub>33</sub>	30.1K, precision
R <sub>34</sub> , R <sub>35</sub>	10K, precision
OA1	Philbrick/Nexus ESL-1

Heat sinks, common; Q<sub>15</sub>, Q<sub>16</sub>

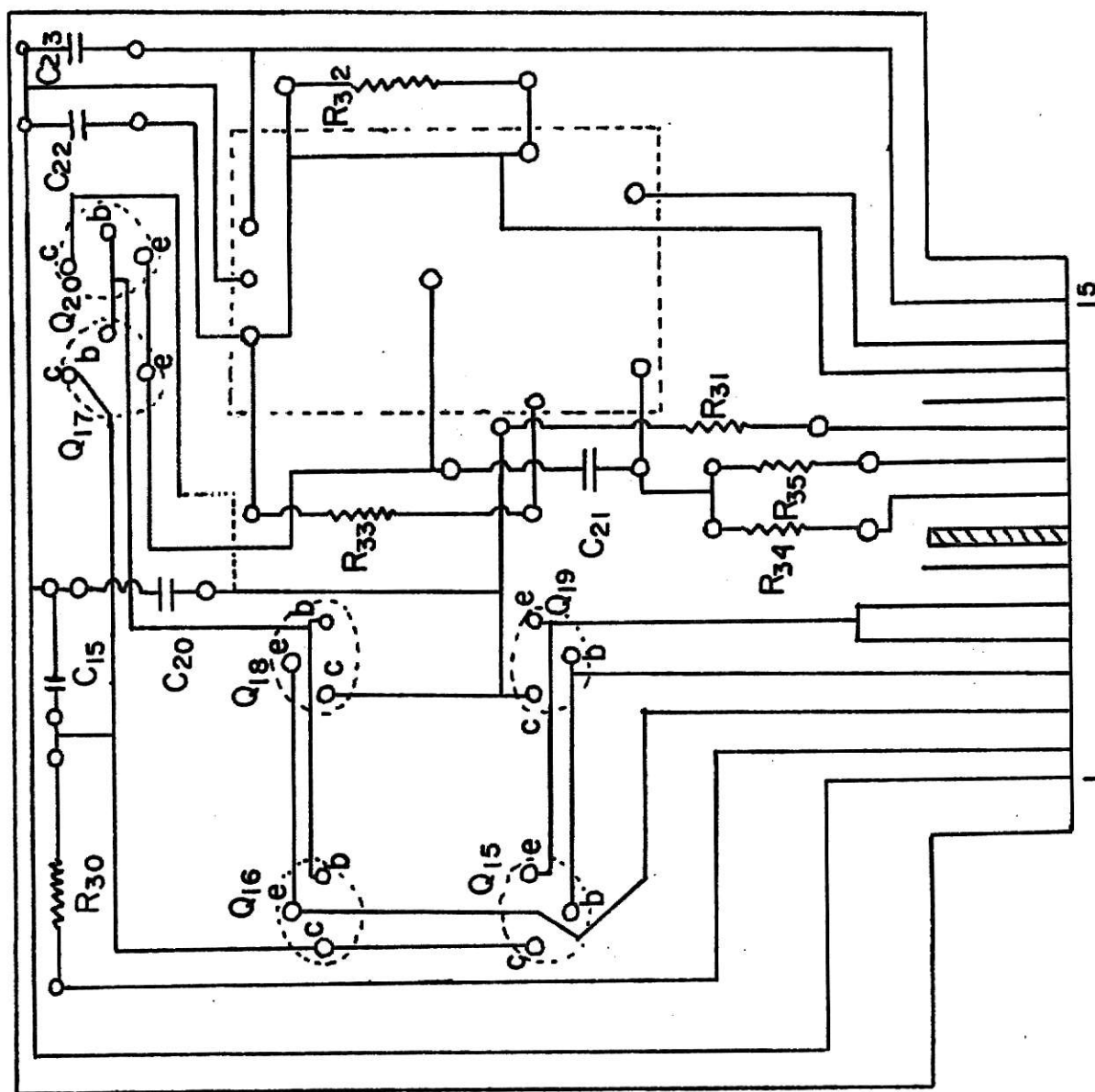
Heat sinks, common; Q<sub>18</sub>, Q<sub>19</sub>

## Current Boosters and Common Mode Rejection Amplifier: (Fig. 18) Board IV

## Socket pin connections:

1	power ground
2	+14 volt dc
3	bridge input
4	clamp
5	N. C.
6	bridge input
7	same as 6
8	key
9	bridge output
10	bridge output
11	-14 volt dc
12	N. C.
13	-15 volt dc
14	signal ground
15	+15 volt dc

Figure 18. The arrangement of the components of Board IV as viewed from the foil side.



ETCH PATTERN BOARD IV, FOIL SIDE

Preamplifier and Demodulator: (Fig. 19) Board V

Parts List:

C <sub>24</sub> , C <sub>25</sub>	220pF
C <sub>26</sub>	1 $\mu$ F
P <sub>9</sub> , P <sub>10</sub>	200 ohm trim potentiometer
Q <sub>21</sub> , Q <sub>22</sub>	3N138
R <sub>36</sub> , R <sub>37</sub>	1K, precision
R <sub>38</sub> , R <sub>39</sub>	100K
R <sub>40</sub> , R <sub>41</sub>	100K
R <sub>43</sub> , R <sub>44</sub>	30.1K, precision
S <sub>3A</sub> , S <sub>3B</sub>	DPDT
T <sub>2</sub>	Triad type G64
OA4	Philbrick/Nexus ESL-1

Preamplifier and Demodulator: (Fig. 19) Board V

Socket pin connections:

1	bridge output
2	bridge output
3	+15 volt dc
4	transformer primary
5	-15 volt dc
6	transformer secondary
7	oscillator
8	N. C.
9	oscillator
10	key
11	transformer secondary
12	N.C.
13	switch $S_{3A}$
14	N. C.
15	power ground

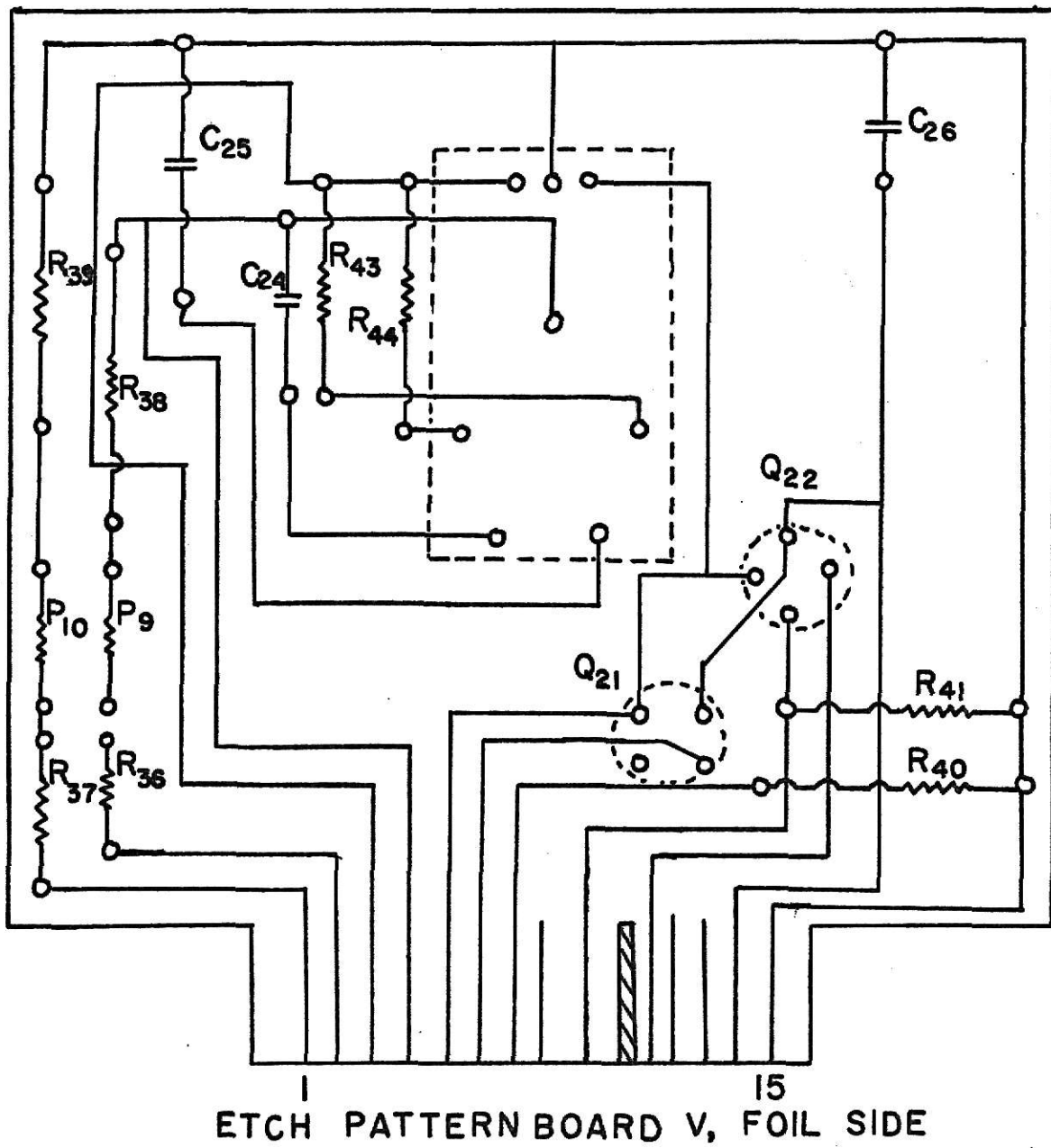


Fig. 19



dc-ac Switching Circuit: (Fig. 20) Board VI

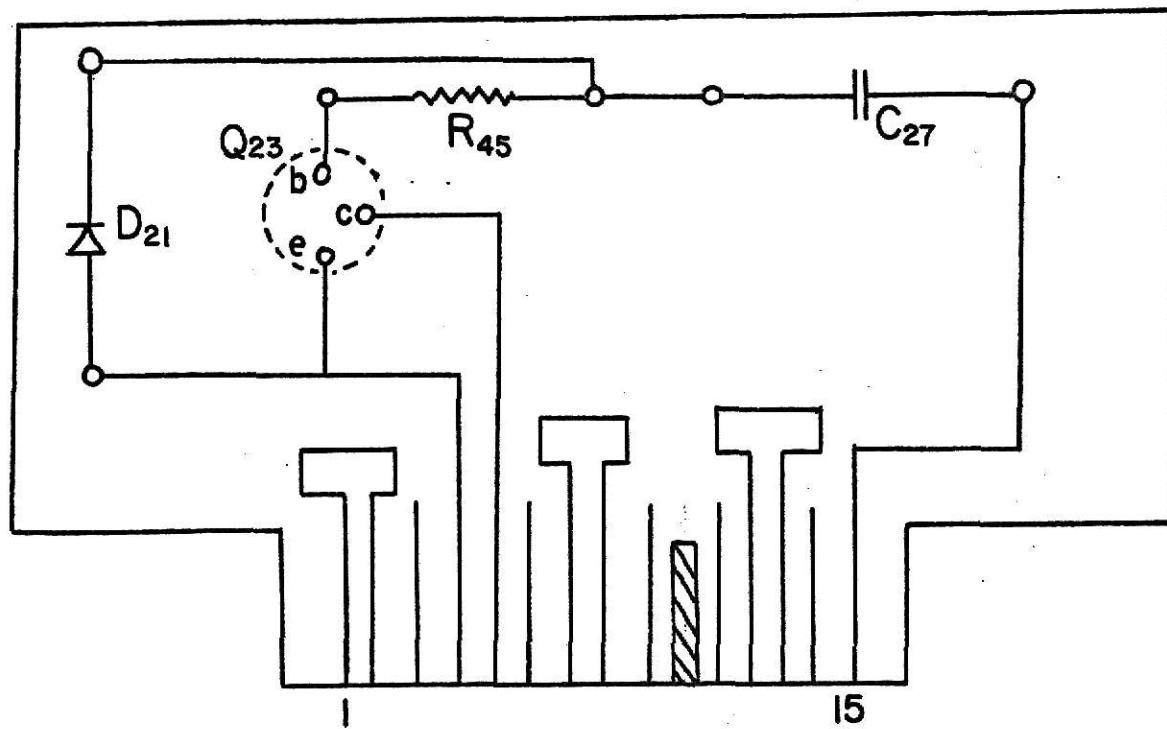
Parts List:

C <sub>27</sub>	.01 $\mu$ F
D <sub>21</sub>	1N34
L <sub>2</sub>	indicator light, 24 volt
Q <sub>23</sub>	2N3417
R <sub>45</sub>	150K
S <sub>2</sub>	SPDT

## dc-ac Switching Circuit: (Fig. 20) Board VI

## Socket pin connections:

1	+36 volt dc
2	L <sub>2</sub> terminal 1
3	N. C.
4	power ground
5	N. C.
6	L <sub>2</sub> terminal 2
7	N. C.
8	-15 volt dc
9	S <sub>2</sub> terminal 1
10	key
11	N. C.
12	S <sub>2</sub> terminal 2
13	P <sub>3</sub> CW terminal
14	N. C.
15	Q <sub>12</sub> emitter



ETCH PATTERN BOARD VI, FOIL SIDE

Fig.20

## Bridge Control Circuit: Fig. 13

## Parts List:

P <sub>11</sub>	500 ohm, 3-turn potentiometer
P <sub>12</sub>	2K trim potentiometer
R <sub>46</sub> , R <sub>57</sub>	10K, precision
R <sub>58</sub>	2K, precision
R <sub>59</sub>	10K, precision

## Attenuator: Fig. 10

## Parts List:

R <sub>47</sub>	0.0220K
R <sub>48</sub>	0.0436K
R <sub>49</sub>	0.1102K
R <sub>50</sub>	0.2208K
R <sub>51</sub>	0.4443K
R <sub>52</sub>	1.101K
R <sub>53</sub>	2.207K
R <sub>54</sub>	4.406K
R <sub>55</sub>	11.00K
R <sub>56</sub>	22.05K

**OPERATION:**

The bridge is connected to the instrument. The power is turned on after the carrier gas is supplied to the gas chromatograph. Horizontal and vertical symmetry, frequency and amplitude of the square-wave are adjusted at a certain voltage within the limits mentioned on page 23 with the aid of an oscilloscope after the carrier gas flow through the gas chromatograph is stabilized.

The current to the bridge is measured by connecting an ammeter between the bridge input and the supply, at 3 or 6 on board IV, while the dc-ac switch is set at dc position.

The system needs about 1-2 hours for warm-up. The main cause for the long warm-up is the establishment of thermal equilibrium in the detector block.

## DATA and DISCUSSION:

The bridge power supply of the Perkin-Elmer Model 900 Gas Chromatograph was disconnected and replaced with our system. No other modifications were made to the chromatograph.

Column	3-foot copper, 1/4" o.d.
Column Packing	5% Squalane on Chromosorb W, mesh size: 60/80
Column system	Dual
Carrier Gas	Helium, industrial purity.
Flow Rate 1	45ml/min.
Flow Rate 2	28ml/min.
Sample 1	air
Sample size 1	10 $\mu$ l
Sample 2	air in helium
Sample size 2	0.02 $\mu$ l air in 10 $\mu$ l helium
Detector Temp.	Room Temperature: 25°C
Bridge Current	275 mA
Bridge Voltage	14 volts, p-p (ac or dc)
Frequency of square-wave ac	1000 cycles per second

The columns are conditioned prior to their use for 8 hours. The columns provide means for a good flow stabilization. A Hamilton-type, #701, 10  $\mu$ l syringe was modified in our laboratory to make it air tight. This syringe was used for the introduction of all samples. A Heath-Kit recorder whose full-scale was set at 3 mV was used; with the preamplifier in our system the recorder full-scale response corresponds approximately to 50  $\mu$ V bridge unbalance.

Since a sensitive thermal conductivity detector will be particularly useful for the detection of permanent gases such as oxygen, nitrogen, carbon dioxide, etc., for which common ionization detectors are insensitive, we decided to evaluate the response of the present system with air samples. The results are summed in Fig. 21. Fig. 21a represents elution of 0.2  $\mu$ l of air in a 10  $\mu$ l sample of helium when the carrier gas flow rate was 28ml/min. and when the bridge was powered with ac current. The peak in Fig. 21b corresponds to a 10  $\mu$ l air sample with dc current. The carrier gas flow rate was 45ml/min. The attenuator was set at X1. The peak in Fig. 21c was obtained with the same sample size, 10  $\mu$ l air, and the flow rate, 45ml/min., but the bridge was powered with ac current, and the attenuator was set at X100. The difference in area under the two peaks, Fig. 21b and c, arises from the loss at demodulation.

The observation of the negligible amount of noise, 20 nanovolts p-p when the output leads of the bridge were shorted shows that the baseline noise of about 300 nanovolts p-p under operating conditions is due largely to inherent noise of the detector block.

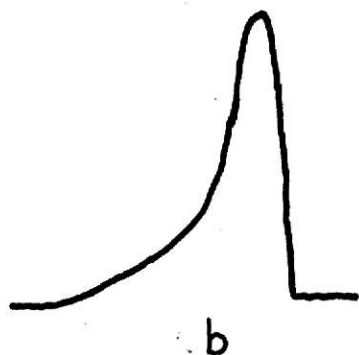
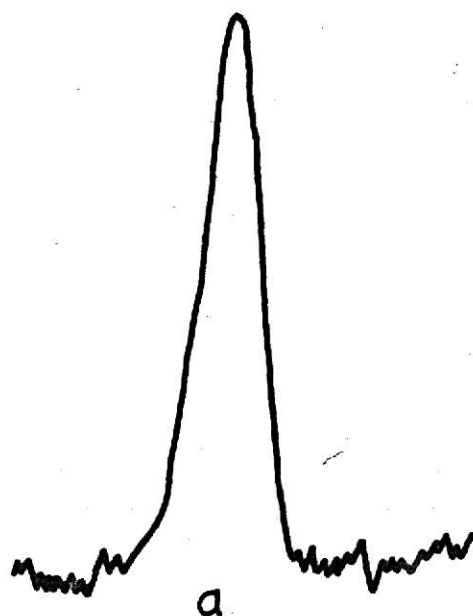
Bridge unbalance signals of the order of 10 nanovolts can be measured with "phase locked" demodulation of the amplified signal. This performance exceeds the requirements of the presently available detector cells which produce noise levels of the order of 100 nanovolts.

The instrument is compatible with most existing hot wire detectors and may be used with economical recorders. Air and other permanent gases can be easily and reliably analyzed at levels of 0.1  $\mu$ l, with detection limits of the order of 0.01  $\mu$ l. It opens up the way to further research in the design of low-level noise detector block.

A C

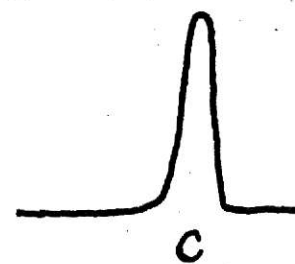
ATTENUATION: XI

SAMPLE SIZE:

.2 $\mu$ l AIR

DC

ATTENUATION: XI



A C

ATTENUATION: X100

SAMPLE SIZE: 10 $\mu$ l AIR

Fig. 21



## REFERENCES:

1. Langmuir, I., Phys. Rev., 34, 401 (1912).
2. Shakespear, G. A., Proc. Phys. Soc. London, 33, 163 (1921).
3. Daynes, H. A., Gas Analysis by Measurement of Thermal Conductivity, Cambridge University Press, London, 1933 p. 51.
4. Claesson, S., Ark. Kemi. Min. Geol., A23, 133 (1946).
5. Johns, T. and Sternberg, J. C., Instrumentation in Gas Chromatography, J. Krugers, Ed., Centrex Publishing Co., Eindhoven, 1968, p. 187.
6. Schmauch, L. J., Dinerstein, R. A. and Ray, L., Nature 183, 673 (1959).
7. King, W. H. Jr., and Dupre, G. D., Anal. Chem., 41, 1936 (1969).
8. Dimbat, M., Porter, P. E. and Stross, F. H., Anal. Chem., 28, 290 (1956).
9. Nogare, S. D., Presented at the ACS Midwest Regional Meeting, at Columbia, Mo. 1967.
10. Coor, T., J. Chem. Ed., 45, A533, A583, (1968).
11. Keulemans, A. I. M., Gas Chromatography, Reinhold, New York, 1959.
12. Ackman, R. G., Burgher, R. D., and Sipos, J. C., J. Chrom., 9, 531 (1962).
13. James, A. T. and Martin, A. J. P., Biochem. J., 50, 679 (1952).
14. Kaiser, R., Gas Chromatography, Vol. I, Butterworth, Washington D. C. 1963.
15. Ongkielong, L., in Gas Chromatography 1960, R. D. Scott, Ed., Butterworths, London, 1960.
16. Nogare, D. S. and Juvet, R. C., Gas Liquid Chromatography, Interscience Publishers, New York, 1962.
17. Scott, B. A. and Williamson, G. A., Nature 183, 1322 (1959).
18. Hoffmann, R. L. and Evans, C. D., J. Gas Chrom., 4, 198 (1966).
19. Conlan, D. A. and Szonntag, H., J. Chrom., 10, 105 (1963).

20. Jessop, G., J. Sci. Inst. 43, 777 (1966).
21. Obermiller, E. L. and Charlier, G. O., Anal. Chem., 39, 397 (1967).
22. Penn, W. H. and Lotz, F. G., U. S. Patent 3,088,310 (1963).
23. Desty, D. H., Nature 180, 22 (1957).
24. Scott, D. S. and Han, A., Anal. Chem., 33, 160 (1961).
25. Soma, S. and Takeuchi, Y., J. Phys. Soc. of Japan 15, 333 (1967).
26. Magnusz, F., Polish Patent 50,147 (1965).
27. Cieplinski, E. W. and Dooley, J. W., Presented at the 153rd ACS Meeting Div. Anal. Chem., Miami Beach, Florida, 1967.
28. Friel, D. D., Ind. Eng. Chem., 52, 494 (1960).
29. Schmauch, L. J., U. S. Patent 3,075,379 (1963).
30. Kieselbach, R., Anal. Chem., 32, 1749 (1960).
31. Modell, M., Anal. Chem., 40, 1444 (1968).
32. Hannah, R. E. and Sontag, R. J., J. Gas Chrom., 5, 384 (1967).
33. Littlewood, B. A., J. Sci. Instr., 37, 185 (1960).
34. Buhl, D., Anal. Chem., 40, 715 (1968).
35. Madden, W. F., Quigg, R. K. and Kemball, C., Chem. Ind. London, 892 (1957).
36. Bennet, E., Nogare, D. S., Safranski, L. W. and Lewis, C., Anal. Chem., 30, 898 (1958).
37. Burg, S. P. and Stolwijk, J. A. J., J. Biochem. Microbio. Tech. Eng., 1, 245 (1959).
38. Furst, H. and Heinzig, E., Chemische Technik, 14, 45 (1962).
39. Grice, H. W. and David, D. J., J. Chrom. Science, 7, 239 (1969).
40. Winefordner, J. D. and Williams, H. P., J. Gas Chrom., 6, 11 (1968).
41. Nalle, D. H., Inst. and Contr. Syst., 42, 77 (1969).

- 42. Bittenbach, R. W., Inst. and Contr. Syst., 42, 135 (1969).
- 43. General Electric Transistor Manual, Ch. 10, p. 231 (1964).
- 44. RCA Transistor Manual, p. 35 (1964).
- 45. Malmstadt, H. V. and Enke, C. G., Electronics for Scientists, W. A. Benjamin Inc., New York, p. 434, 1962.
- 46. Golden, F. B., Electronics, 41, 82 (1968).
- 47. Fairchild Linear Integrated Micro Circuits,  $\mu$ A709C.
- 48. RCA Semiconductors and Integrated Circuits, File #283.

**ACKNOWLEDGEMENT:**

I would like to thank my research advisor, Dr. Maarten van Swaay, for his encouragement and guidance throughout my study, for his introduction to the theoretical and the practical aspects of electronics, for his friendship and for his translations of numerous papers pertaining to my work from German, French and Dutch.

I would like to acknowledge Rowan Conrad's work in the development of the regulated power supply and also Gene Rugotzke's constructive criticisms.

I would also like to thank Perkin-Elmer Company for making available a Perkin-Elmer Model 900 Gas Chromatograph for the work.

## VITA:

March 6, 1943	Born at Ankara, Turkey to Mehmet Ali and Mualla Ediz.
1950-1952	Sakarya Elementary School at Adapazari.
1952-1953	Gemlik Elementary School at Gemlik.
1953-1955	Gazi Mustafa Kemal Elementary School at Kadikoy, Istanbul.
1955-1956	Maarif Koleji Prep School at Moda, Istanbul.
1956-1962	Maarif Koleji Junior and Senior High School at Moda, Istanbul.
1962-1963	Manhasset Public High School, Manhasset, New York.
1963-1967	Wabash College, Crawfordsville, Indiana. Received B. S.
1967-1970	Graduate Teaching Assistant at Kansas State University, Manhattan, Kansas.

SQUARE-WAVE OPERATION OF A THERMAL CONDUCTIVITY DETECTOR

by

SUNTAY HAYRI EDIZ

B. S., Wabash College, 1967

---

AN ABSTRACT OF A MASTER'S THESIS

submitted in partial fulfillment of the

requirements for the degree

MASTER OF SCIENCE

Department of Chemistry

KANSAS STATE UNIVERSITY  
Manhattan, Kansas

1970

# ABSTRACT:

Conventional thermal conductivity detectors in gas chromatography are powered with dc current. The bridge unbalance signal, which may be as small as a few microvolts, is handled by the use of chopper-stabilized amplifiers, e.g. the servo amplifier which is a part of most potentiometric recorders. To remove the drawbacks of dc amplification of low-level signals, we have designed a bridge operated with ac power which allows ac amplification of the unbalance signal without the need for a chopper operating on a low-level signal. The bridge output is of known phase and of known frequency, so random noise can be removed by a phase-locked demodulator. The instrument designed on the basis of these arguments achieves a lower detection limit.

If varying current is applied to the elements of the bridge, problems such as thermal vibrations and magnetic interactions between the loops of the filaments may arise. Such effects may not only damage the filaments, but may also give rise to thermal noise. If the voltage supplied to the bridge is sinusoidal ac, power will vary as a function of time, since power is directly proportional to the square of the current.

To eliminate the problems mentioned above, a perfectly symmetrical square-wave ac should be applied. This will result in constant power at the filaments at all times. The vertical symmetry of the square-wave is crucial.

Nearly all of the components of our solid-state instrument are mounted on six 4" x 4" copper plated circuit boards. The boards contain a regulated power supply, smoothed high current supply, oscillator and clamps, common mode rejection amplifier and booster amplifiers, preamplifier and demodulator, and dc-ac switching system.

Performance of the instrument was evaluated with air samples of 0.2  $\mu$ l-

10  $\mu$ l. All injections of sample were made with a 10  $\mu$ l air-tight syringe. The bridge was powered with ac and dc currents respectively. The peaks obtained are in the ratio of 85:1. The gain of the amplifier after the bridge was set at 100. The 15% loss of the signal is due to demodulation.

The 300-nanovolt p-p noise on the baseline under operating conditions is due largely to inherent noise of the detector block, e.g. when the output leads of the bridge are shorted the baseline noise is of the order of 20 nanovolts p-p.

Bridge unbalance signals of the order of 10 nanovolts can be measured with phase-locked demodulation of the amplified signal. This performance exceeds the requirements of the presently available detector cells which produce noise levels of the order of 100 nanovolts. The instrument is compatible with most existing hot wire detectors, and may be used with economical recorders.